International Tables for Crystallography (2006). Vol. C, Chapter 7.1, pp. 618–638.

7.1. Detectors for X-rays

BY Y. AMEMIYA, U. W. ARNDT, B. BURAS, J. CHIKAWA, L. GERWARD, J. I. LANGFORD, W. PARRISH AND P. M. DE WOLFF

7.1.1. Photographic film*

In 1962, when Volume III of *International Tables for X-ray Crystallography* was published, photographic film was the commonest detector for X-rays. Now it has been largely supplanted by the electronic devices described in other sections, but it is still much used in powder cameras and in preliminary investigation of specimens.

X-rays and other radiations cause blackening of silver halide emulsions, and their intensity can be measured accordingly. The blackening of the film is expressed in units of density:

$$D = \log_{10} (\mathscr{I}_{\text{incident}}/\mathscr{I}_{\text{transmitted}}), \qquad (7.1.1.1)$$

where $\mathscr{I}$ refers to the intensity of the ordinary light incident on the film. Measured densities must be corrected by subtracting the fog density D_F measured on a non-exposed part of the film.

Important features of the photographic process for strongly ionizing radiations such as X-rays and electrons are:

(i) For a given total exposure E the relationship between D and E is, to a close approximation, independent of the time variation of the intensity of the incident radiation. It does not matter whether the X-ray quanta arrive continuously or in short intense bursts (Mees, 1954).

(ii) The density D increases linearly with E up to $D \simeq 1$, then increases more slowly.

Photographic intensity measurements may be made either visually or by using a microdensitometer.

7.1.1.1. *Visual estimation*

Visual estimation consists of comparing the spot or line to be measured with a series of exposure-calibrated marks similar in shape to the object of measurement, and preferably made with the same specimen and incident beam. Lack of complete similarity and unfavourable background usually cause the error of such measurements to be larger than the optimum contrast threshold of the eye. For a spot area of 1 mm^2, the latter amounts to roughly 1% or 0.004 density units, a difference that can in fact be detected under favourable circumstances (low density and low background).

7.1.1.2. *Densitometry*

If the blackening is measured with a microdensitometer, an accuracy of 0.002 density units up to densities of at least 2 is easily attained. Higher precision is rarely required, as the limiting factors are graininess of the film and irregularities in the emulsion and processing. The grains in processed X-ray film are larger than those produced by visible light, and occur in clusters around each absorbed quantum. The resulting statistical fluctuations may be minimized by appropriate choice of densitometer slit dimensions and scanning speed. If the X-rays are not incident normally on double-coated film, it may be necessary to make corrections for obliquity (Whittaker, 1953; Hellner, 1954).

* Editorial condensation of the entry by P. M. de Wolff in Chapter 3.1 of Volume III.

7.1.2. Geiger counters†

Geiger-Müller counters (Geiger & Müller, 1928) are now obsolete for data collection, but are still used in portable monitors for X-rays. A cross section of a once-popular type is shown in Fig. 7.1.2.1(*a*). The cathode *C* is a cylinder made of a metal such as chrome-iron, about 2 cm in diameter and 10 cm long. The anode *A* is a tungsten wire about 0.7 mm in diameter mounted coaxially with *C* and terminated by a bead to prevent destructive electrical discharges from its tip. About 1400 V DC is applied between *C* and *A*. X-rays enter at a low-absorption end window *W*, made of mica about 0.013 mm thick or other suitable material; beryllium would now be used. The gas filling may be argon at a pressure of about 55 cm Hg or krypton at a lower pressure. A small amount of halogen (~0.4% of chlorine or bromine) helps to avoid destructive discharges. Separating the anode and the window is a dead space in which X-rays are absorbed but not detected.

The quantum-counting efficiency varies with wavelength; for Cu K and its neighbours, it is about 50% and, for Mo K, it is about 10%. For the longer wavelengths, it is limited by absorption in the window and the dead space, so it is important to keep these as thin as practicable. For the shorter wavelengths, it is limited by the transparency of the gas in the sensitive volume.

† Editorial condensation of the entry by W. Parrish in Chapter 3.1 of Volume III. Several papers on the relative advantages of various detectors are collected in Parrish (1962). Sections 7.1.2–7.1.4 have been slightly revised by J. I. Langford.

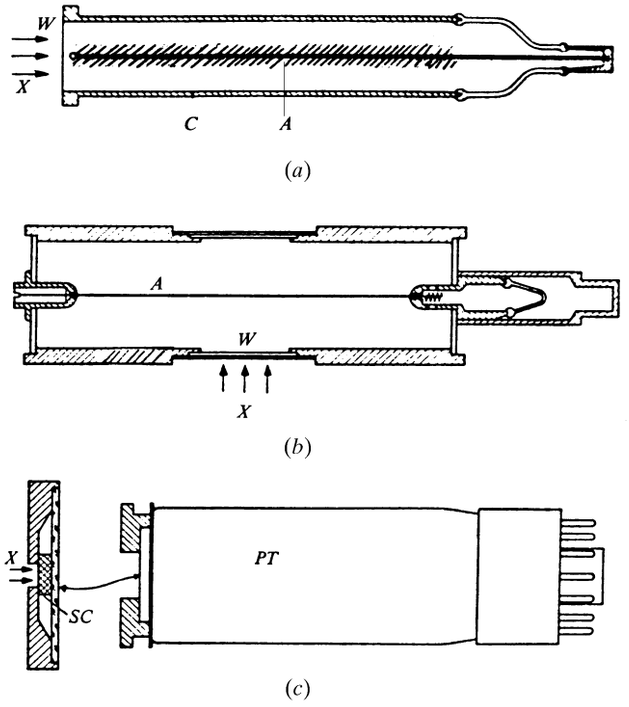

Fig. 7.1.2.1. Detectors used for diffractometry: (*a*) Geiger counter, (*b*) side-window proportional counter, (*c*) end-window scintillation counter. The arrows *X* show direction of incident X-ray beam, *W* thin window, *C* cathode, *A* anode, *SC* scintillation crystal, *PT* photomultiplier tube.

The tube is not uniformly sensitive across its diameter. The maximum sensitivity is confined to the cylindrical volume shown cross-hatched in the figure. The diameter of this sensitive area depends on the gas filling and the geometry of the tube. For maximum efficiency, the X-ray beam should be directed along and close to the anode, but should not strike it. Geiger counters are not critically temperature-dependent. Linearity of response is limited by the dead-time following the discharge initiated by the absorption of a quantum and the magnification of the few hundred ions produced to some millions by their acceleration under the electric field. To produce this amplification, a certain minimum threshold voltage is required. Above this minimum, there is a plateau extending for several hundred volts within which the number of quanta detected is essentially independent of the applied voltage and the size of the pulses is essentially independent of the energy of the absorbed quantum.

Geiger counters are simple to use and show little deterioration even after prolonged use. However, since the pulses are all of about the same size, pulse-height discrimination cannot be used, and the long dead-time limits linearity of response unless special monitoring circuits are used (Eastabrook & Hughes, 1953). They have been almost completely superseded by other types of counter, described in Sections 7.1.3.–7.1.8.

7.1.3. Proportional counters (By W. Parrish)

7.1.3.1. *The detector system*

The commonest types of detector for both powder and single-crystal diffractometry are proportional counters and especially scintillation counters (Section 7.1.4). The detector system consists of the detector itself, a high-voltage power supply, a single-channel pulse-height analyser, and a scaling circuit, as shown schematically in Fig. 2.3.3.5. For position-sensitive detectors (Section 7.1.3.3) and solid-state detectors (Sections 7.1.4.2 and 7.1.5), multichannel analysers are necessary. The X-ray manufacturers and a number of electronic companies provide complete detector systems, often integrated with the computer data-collection system.

7.1.3.2. *Proportional counters*

Proportional counters are available in various sizes and gas fillings. A typical detector is a metal cylinder about 2 cm in diameter and 8–10 cm long, with central wire anode and 0.13 mm Be side window, Fig. 7.1.2.1(*b*). Some have an opposite exit window to transmit the unabsorbed beam and thus avoid fluorescence from the wall. The tube may be filled with Xe to atmospheric pressure for high absorption, and a small amount of quenching gas such as CO_2 or CH_4 is added to limit the discharge. When an X-ray quantum is absorbed, the discharge current is the sum of the Townsend avalanches of the secondary electrons and the gas amplification is about 10^4. A charge-sensitive preamplifier is generally used. Some proportional counters are filled to several atmospheres pressure to increase the gas absorption. Very thin organic film windows are used for very long wavelengths as in fluorescence spectroscopy. They may transmit moisture, and gas may migrate through them so that flow counters are used to replenish the gas. This requires careful control of the pressure to avoid changes in the counting efficiency.

7.1.3.3. *Position-sensitive detectors*

One variety of position-sensitive detector, in which the photon absorptions in different regions are counted separately, is a special type of proportional counter. The following description applies primarily to one-dimensional detectors for powder diffractometry; two-dimensional (area) detectors are treated in Section 7.1.6.

Position-sensitive detectors (PSD's) are being used in increasing number for various powder-diffraction studies. They have the great advantage of simultaneously recording a much larger region of the pattern than conventional counters. The difference in receiving apertures determines the gain in time. The position at which each quantum is detected is determined electronically by the system computer and stored in a multi-channel analyser. There is a digital addition of each incident photon address and the angular address of the diffractometer.

The PSD's are available in short straight form and as longer detectors with curvature to match the diffractometer focusing circle. The short detectors can be used in a stationary position to cover a small angular range or scanned. Göbel (1982) developed a high-speed method using a short (8° window) scanning PSD with 50 μm linear resolution in the diffractometer geometry shown in Fig. 2.3.1.12(*b*). He was able to record at speeds of a hundred or more degrees a minute, and patterns with reasonably good statistical precision in several tens of degrees a minute. This is faster than conventional energy-dispersive diffraction and has the advantage of much higher resolution.

The PSD should be selected to match best the diffraction geometry. The detector is sensitive across the 1–2 cm gas-absorption path. If the diffracted rays are not perpendicular to the window, the parallax causes broadening and loss of resolution. This becomes important in the focusing geometries and can be minimized if the diffractometer and specimen focusing circles are nearly coincident. A large loss of resolution would occur in the conventional geometry, Fig. 2.3.1.3, because only the central ray of a single reflection would be normal to the window. The problem is minimized in powder-camera geometry with a thin rod specimen, Fig. 2.3.4.1(*a*), where the entire pattern can be recorded with a long, curved PSD (Ballon, Comparat & Pouxe, 1983); see also Shishiguchi, Minato & Hashizume (1986), Lehmann, Christensen, Fjellvåg, Feidenhans'l & Nielsen (1987), Wölfel (1983), and Foster & Wölfel (1988).

7.1.3.4. *Resolution, discrimination, efficiency*

The topics of energy resolution, pulse-height discrimination, quantum-counting efficiency, and linearity are common to proportional, scintillation and solid-state counters, and are treated in Subsections 7.1.4.3.–7.1.4.5.

7.1.4. Scintillation and solid-state detectors (By W. Parrish)

7.1.4.1. *Scintillation counters*

The most frequently used detector is the scintillation counter (Parrish & Kohler, 1956). It has two elements: a fluorescent crystal and a photomultiplier tube, Fig. 7.1.2.1(*c*). For X-ray diffraction, a cleaved single-crystal plate of optically clear NaI activated with about 1% Tl in solid solution is used. The crystal is hygroscopic and is hermetically sealed in a holder with thin Be entrance window and glass back to transmit the visible-light scintillations. The size and shape of the crystal can be selected, but is usually a 2 cm diameter disc or a rectangle $20 \times 4 \times 1$ mm thick. A small thin crystal has been used to reduce the background from radioactive samples (Kohler & Parrish, 1955). A viscous mounting fluid with about the same refractive index as the glass is used to reduce light reflection and to attach it to the end of the photomultiplier tube. The crystal and

photomultiplier are mounted in a light-tight cylinder surrounded by an antimagnetic foil. The high X-ray absorption of the crystal provides a high quantum-counting efficiency.

A Cu $K\alpha$ quantum produces about 500 visible photons of average wavelength 4100 Å in the scintillation crystal (which matches the maximum spectral sensitivity of the photomultiplier), but only about 25 will be effective in the photomultiplier operation. High-speed versions with special pulse-height analysers have recently become available; they are linear to about 1% at 10^5 counts s^{-1} and can be used at rates approaching 10^6 counts s^{-1} (see Rigaku Corporation, 1990).

The detector system is as described in Subsection 7.1.3.1.

7.1.4.2. *Solid-state detectors*

The following description applies primarily to the use of solid-state detectors in powder diffractometry. Further details of their operation and their use in energy-dispersive diffractometry are treated in Section 7.1.5.

The most common form of solid-state detector consists of a lithium-drifted silicon crystal Si(Li) and liquid-nitrogen Dewar. A perfect single crystal is used with very thin gold film on the front surface for electrical contact. The first amplifier stage is a field-effect transistor (FET). The unit must be kept at liquid-nitrogen temperature at all times (even when not in use) to prevent Li diffusion and to reduce the dark current when in use. The unit is large and heavy and, if not used in a stationary position, a robust detector arm is required, which is usually counter-balanced. The crystal is made with different-size sensitive areas and the resolution is somewhat dependent on the size of the area. In the detector process, the number of free charge carriers (the electron and electron–hole pairs) generated during the X-ray absorption changes the conductivity of the crystal and is proportional to the energy of the X-ray quantum. Details of the mechanism are given in several books [see, for example, Heinrich, Newbury, Myklebust & Fiori (1981) and Russ (1984)].

Intrinsic germanium detectors have higher absorption than silicon detectors, but they have lower energy resolution and there are more interferences from escape peaks. A mercuric iodide (HgI_2) detector can be operated at room temperature and has high absorption (Nissenbaum, Levi, Burger, Schieber & Burshtein, 1984). They have poorer resolution than Si or Ge detectors but can be improved to FWHM = 200 eV at 5.9 keV by cooling to 269 K (Ames, Drummond, Iwanczyk & Dabrowski, 1983).

A small (about 16.5×10 cm), lightweight (3.2 kg) silicon detector with Peltier thermoelectric cooling is available (*e.g.* Kevex Corporation, 1990). This development has supplanted a number of the methods of collecting powder data. The elimination of the liquid-nitrogen Dewar and the compact size makes it possible to replace conventional detectors and the diffracted-beam monochromator in scanning powder diffractometry. The spectrum is displayed on a small screen and the window of the analyser can be set closely on the energy distribution obtained from a powder reflection to transmit, say, only Cu $K\alpha$. The monochromator can be eliminated for a large gain of intensity without loss of pattern resolution. The energy resolution is FWHM $\approx$ 195 eV at 5.9 keV. Elemental analysis can be performed by energy-dispersive fluorescence, and the background can be restricted to the narrow energy window selected. Bish & Chipera (1989) used it to obtain a 3–4 times increase of intensity, the same pattern resolution, and lower tails than with a graphite monochromator and scintillation counter in conventional diffractometry. The major limitation at present is the limited input intensity that can be handled. The limiting (total) count rate is about 10^4 counts s^{-1} and the detector becomes markedly nonlinear at 2×10^4 counts s^{-1}. Internal dead-time corrections can extend the range by increasing the counting times.

7.1.4.3. *Energy resolution and pulse-amplitude discrimination*

The pulse amplitudes are proportional to the energy e of the absorbed X-ray quantum so that electronic methods can be used to reduce the background from other wavelengths and sources. The rejection range is limited by the energy resolution of the detector. As noted above, the pulse amplitudes have distributions that vary around the average value A, Figs. 7.1.4.1(*a*),(*b*). The FWHM of the distribution increases linearly with increasing e (eV) and is proportional to $e^{1/2}$, *i.e.* it improves inversely with $\lambda^{1/2}$. The ratio FWHM/A (expressed in %) is a measure of the energy resolution at a given wavelength; the smaller the ratio the better the resolution. For example, as e increases from 5 to 45 keV, the FWHM approximately doubles while FWHM/e decreases from 5 to 1%. The resolution of proportional counters is about 18% for Cu $K\alpha$ and somewhat better for high-pressure gas fillings; in scintillation counters, it is about 45%. The solid-state detectors have much better resolution. The best are about 2.4% (145 eV) at 5.9 keV (which is the energy of Mn K X-rays from a radioactive ^{55}Fe source used as a standard for calibration).

The electronics include a high-voltage power supply to about 1200 V for scintillation counters and 2000–3000 V for proportional counters, and a single-channel pulse-amplitude discriminator. The latter contains pulse-shaping circuits and the amplifier, and is designed to transmit pulses whose amplitudes lie within the selected range. The lower level rejects all pulses below the selected level and the upper level rejects the higher amplitudes (Figs. 7.1.4.1*a*, *b*). The range selected is called the window and determines the pulse amplitudes that will be counted by the scaling circuit.

The multichannel analyser is generally used with solid-state detectors. It may have up to 8000 channels and sorts the pulses from the amplifier into individual channels according to their amplitudes, which are proportional to the X-ray photon energies. The pattern can be stored and displayed on a CRT screen, but nowadays a personal computer with a suitable interface card is normally used in place of the analyser. Various programs are available for peak-energy identification, spectral stripping, intensity determination, and similar data-reduction requirements. The limiting count rate that can be handled by the electronics is determined by the total number of photons striking the detector. Pulse-pileup rejectors are used to stop counting momentarily when another pulse is too close in time to allow the original pulse to return to the baseline voltage. A live-time correction extends the counting period beyond the clock time to compensate for the time the analyser is gated off. About 50 000 counts s^{-1} is the maximum rate so that the individual powder reflections have a much smaller number of pulses. If good statistical accuracy is required, the count times are, therefore, much longer than in conventional diffractometry.

For a given e, the pulse amplitudes of scintillation and proportional counters increase with increasing voltage (internal gain) and amplifier setting (external gain). The detector must be operated in the plateau region for the wavelength used (Fig. 7.1.4.1*c*). The counts are measured as a function of the voltage and/or gain, and the plateau begins where there is no further significant increase of intensity. In selecting the operating

conditions, one should avoid excessively high voltages and amplifier gains, which may cause noise pulses and unstable operation. Optimum settings can be determined by experiment and from manufacturer's instructions. The average pulse height should be set at about 20–25% of the full range of the pulse-height analyser. Lower settings move the low-energy tail into the noise, and high settings broaden the distribution and may be too wide for the window.

The pulse-amplitude distribution can be measured with a narrow (1–3 V) upper level and increasing the lower level by small equal steps. When making this calibration, it is advisable to keep the incident count rate below 10^4 counts s^{-1} to avoid nonlinearity and pulse pileup. A plot of intensity *versus* lower-level setting shows the distribution, Fig. 7.1.4.1(*a*). In some electronics, this can be done automatically and displayed on a screen. The window should be set symmetrically around the peak with the window decreasing the characteristic line intensity only a few per cent below that obtained with the lower-level set to remove only the circuit noise. The intensity change can be seen with a rate meter. Narrow windows cause a larger percentage loss of intensity than the decrease in background and, hence, the peak-to-background ratio is reduced. Asymmetric windows are sometimes used to decrease the fluorescence background.

7.1.4.4. *Quantum-counting efficiency and linearity*

The quantum-counting efficiency E of the detector, its variation with wavelength, and electronic discrimination determine the response to the X-ray spectrum. E is determined by

$$E = f_T f_A, \tag{7.1.4.1}$$

where f_T is the fraction of the incident radiation transmitted by the window (usually 0.013 mm Be) and f_A is the fraction absorbed in the detector (scintillation crystal or proportional-counter gas). E varies with wavelength as shown in Fig. 7.1.4.1(*d*). The scintillation counter has a nearly uniform E approaching 100% across the spectrum and detects the short-wavelength continuous radiation with about the same efficiency as the spectral lines. The gas-filled counters have a lower E for the short wavelengths and, therefore, may have a slightly lower inherent background; high-pressure gas counters have a higher and more uniform spectral efficiency.

The effectiveness of electronic discrimination with a scintillation counter is shown in Fig. 2.3.5.3(*c*) for 50 kV Cu target radiation. The method cannot separate the $K\alpha$-doublet components because of their small energy difference, and has little effect on the $K\beta$ peak. The results are greatly enhanced by the addition of a $K\beta$ filter, which removes most of the $K\beta$ peak and a portion of the continuous radiation below the filter absorption

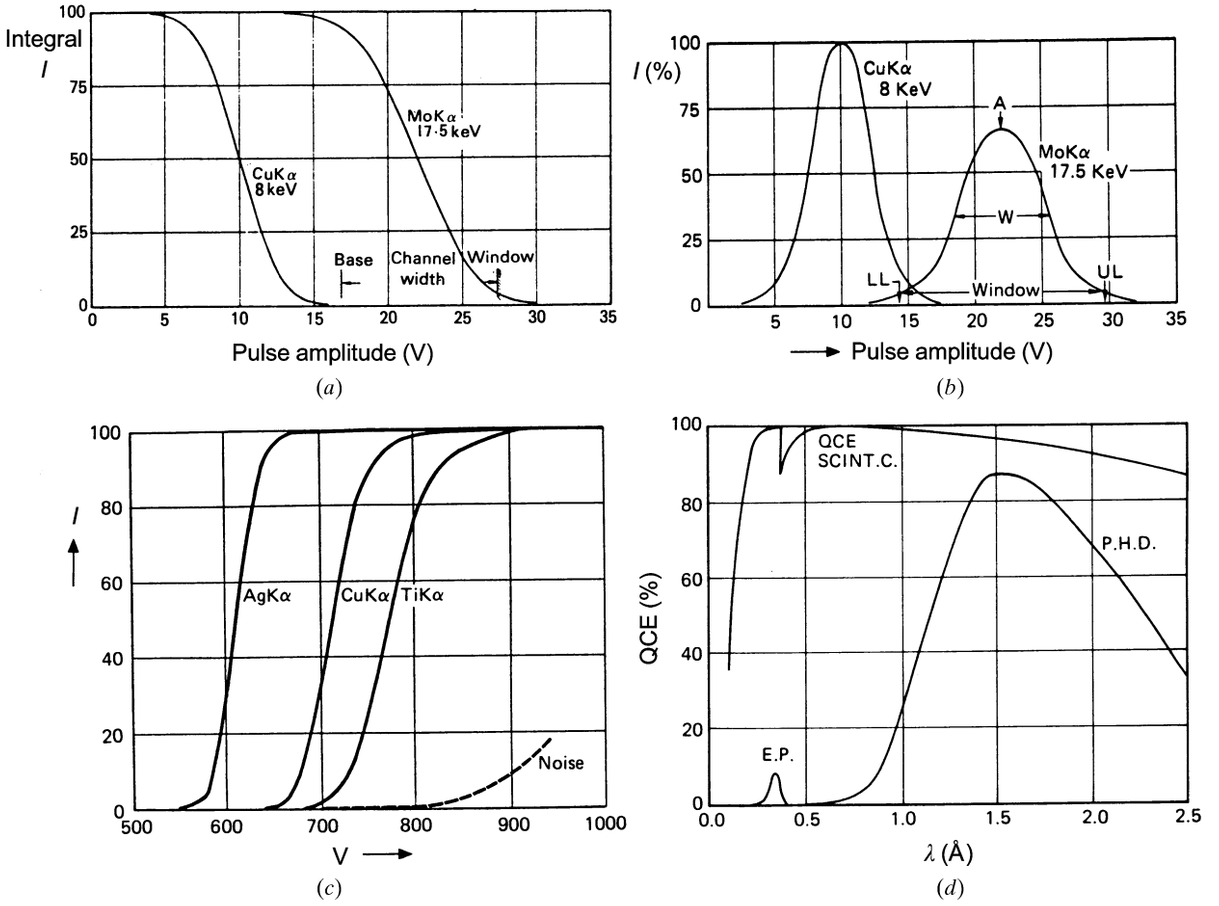

Fig. 7.1.4.1. Calculated pulse-amplitude distributions of Cu $K\alpha$ and Mo $K\alpha$ in the form of (*a*) integral curves and (*b*) differential curves. Resolution W/A for Cu $K\alpha = 50\%$. Analyser settings show window between lower level (*LL*) and upper level (*UL*). (*c*) Plateaux of scintillation counter for various wavelengths and fixed amplifier gain. Curves normalized to same intensity at highest voltage. Noise curve is plotted in counts s^{-1}. Curves can be moved to higher or lower voltages by changing amplifier gain. (*d*) Calculated quantum-counting efficiency (QCE) of scintillation counter as a function of wavelength (top curve) and its reduction when the pulse-height analyser is set for 90% Cu $K\alpha$. E.P. is escape peak at lower left.

edge, Fig. 2.3.5.3(*b*). The combination of discrimination and filter produces mainly the $K\alpha$ doublet, Fig. 2.3.5.3(*d*). Spectral analysis of the background of a non-fluorescence powder sample using this method with 50 kV Cu radiation and a scintillation counter shows it to be 50–90% characteristic radiation.

The linearity of the system is determined by the dead-time of the detector, and the resolving times of the pulse-height analyser and scaling circuit. The observed intensity n_{obs} is related to the effective dead-time of the system τ_{eff} by the relation

$$n_{true} = n_{obs}/(1 - \tau_{eff}\, n_{obs}). \qquad (7.1.4.2)$$

The value of τ_{eff} can be measured with an oscilloscope, or with the multiple-foil method in which a number of equal absorption foils (*e.g.* Al 0.025 mm or Ni 0.018 mm for Cu $K\alpha$) are inserted in the beam one or two at a time. To make certain monochromatic radiation is used, a single-crystal plate such as Si(111), which has no significant second order, and low X-ray tube voltage are employed. The linearity is determined from a regression calculation. A less accurate method is to plot n_{obs} on a log scale against the number of foils on a linear scale. Recent developments in high-speed scintillation counters have extended the linearity to the 10^5–10^6 counts s^{-1} range.

7.1.4.5. *Escape peaks*

The pulse-amplitude distribution may have two or more peaks, even when monochromatic X-rays are used (Parrish, 1966). Absorption of the incident X-rays by the counter-tube gas or scintillation crystal may cause X-ray fluorescence. If this is re-absorbed in the active volume of the counter only one pulse is produced of average amplitude A_1 proportional to the incident X-ray quantum energy e_1 (k = constant)

$$A_1 = ke_1. \qquad (7.1.4.3)$$

However, the gas or crystal has a low absorption coefficient for its own fluorescent radiation, hence, some quanta of the latter of energy e_2 may escape from the active volume of the counter, the amount depending on the geometry of the tube, gas, windows, *etc*. The average amplitude A_2 of the escape pulses is

$$A_2 = k(e_1 - e_2). \qquad (7.1.4.4)$$

Thus,

$$A_1 - A_2 = ke_2. \qquad (7.1.4.5)$$

The pulse-height analyser discriminates against pulses only on the basis of their amplitudes. When it is set to detect X-rays of energy e_0, it is also sensitive to X-rays of energy $e_0 + e_2$. For example, when using an NaI scintillation counter for Cu $K\alpha$, $e_0 = 8$ keV, and for the escape X-rays I $K\alpha$, $e_2 = 28.5$ keV. A pulse-height analyser set to detect X-rays of energy 8 keV is also sensitive to X-rays of energy 36.5 keV, because, from equations (7.1.4.3) and (7.1.4.4),

$$A_0 = k.8 = k(36.5 - 28.5) = A_2. \qquad (7.1.4.6)$$

In Figs. 2.3.5.3(*c*), (*d*) and 7.1.4.1(*d*), the escape peak E.P. shows clearly at 0.35 Å, the wavelength of 36.5 keV X-rays. There may be a number of weak escape peaks arising from the stronger powder reflections. In practice, the escape peak should not be confused with a small-angle reflection. It can be tested by reducing the X-ray tube voltage to below the absorption-edge energy of the element in the detector from which it arises.

7.1.5. Energy-dispersive detectors (By B. Buras and L. Gerward)

In white-beam energy-dispersive X-ray diffraction, the spectral distribution of the diffracted beam is measured either with a semiconductor detector (low-momentum resolution) or with a scanning-crystal monochromator (high-momentum resolution) (see Subsection 2.5.1.3). Commercially available detectors are made of lithium-drifted silicon or germanium [denoted Si(Li) and Ge(Li), respectively], or high-purity germanium (HPGe). There are, however, other materials that are good candidates for making energy-dispersive detectors.

The semiconductor detector can be regarded as the solid-state analogue of the ionization chamber. Charge carriers of opposite sign (electrons and holes) are produced by the X-ray photons. They drift in the applied electric field of the electrodes and are converted to a voltage pulse by a charge-sensitive preamplifier. The energy required for creating an electron–hole pair is 3.9 eV in silicon and 3.0 eV in germanium. The number of electron–hole pairs is proportional to the energy of the absorbed photon (the intrinsic efficiency is discussed below). There is no intrinsic gain and one has to rely on external amplification. The preamplifier employs an input field-effect transistor (FET), cooled in an integral assembly with the detector crystal in order to reduce thermal noise. Usually the detector is operated at liquid-nitrogen temperature. However, Peltier-cooled silicon detectors are available, removing the maintenance concerns of cryostat cooling. The basic counting system consists further of an amplifier, producing a near-Gaussian pulse shape, and a multichannel pulse-height analyser. It is common to use an

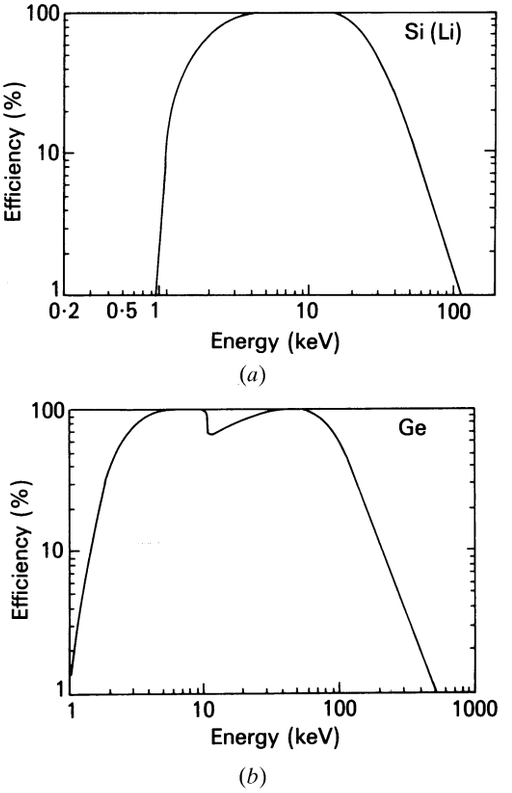

Fig. 7.1.5.1. Intrinsic efficiency of semiconductor detectors. The dimensions are selected to give typical best values of the energy resolution. (*a*) Si(Li), detector thickness 3 mm, Be-window thickness 25 μm. (*b*) HPGe, detector thickness 5 mm, Be-window thickness 50 μm.

additional circuit to reject pileup pulses that can distort the spectrum at high count rates.

The intrinsic efficiency, defined as the ratio of the number of pulses produced to the number of photons striking the detector, is close to 100% in a large energy range. Because of the penetrating power of high-energy X-rays, the efficiency declines at high energies. The low-energy limit is set mainly by the absorption in the beryllium entrance window of the detector. Fig. 7.1.5.1 shows the intrinsic efficiency for an Si(Li) detector and HPGe detector with typical crystal size and window thickness. It is seen that the useful photo-energy range is about 1–40 keV for the Si(Li) detector and 2–150 keV for the HPGe detector. Some minor complications of the HPGe detector are a dip in efficiency around the germanium K absorption edge at 11 keV and the presence of Ge $K\alpha$ and $K\beta$ escape peaks in the measured spectrum.

The energy resolution is commonly expressed as the full width at half-maximum (FWHM) of a peak in an energy spectrum. For a spectral peak with Gaussian shape, ΔE(FWHM) corresponds to 2.355 times the root mean square of the energy spread. The energy resolution, including both the detector and the associated electronics, is given by

$$\Delta E_{\rm FWHM} = \{e_n^2 + [2.355(F\varepsilon E)^{1/2}]^2\}^{1/2}, \qquad (7.1.5.1)$$

where e_n is the electronic noise contribution, F the Fano factor (about 0.1 for both silicon and germanium), and ε the energy required for creating an electron–hole pair.

The energy resolution is generally specified at 5.9 keV (Mn $K\alpha$) as a reference energy. Typical best values for a detector with 25 mm^2 area are 145 eV (2.5%) for an HPGe detector and 165 eV (2.7%) for an Si(Li) detector. The resolution is degraded for larger detector areas.

Count-rate limitations are particularly obvious in synchrotron-radiation applications, where high photon fluxes are encountered (Worgen, 1982). The count rate is limited to below 10^5 counts s^{-1}, mainly by the pulse processing system.

Cadmium telluride, mercury iodide and other wide-band-gap semiconductors could be good candidates for energy-dispersive room-temperature X-ray detectors. Until now, the best energy resolution of the Hg_2I spectrometer with both the detector and the preamplifier operating at room temperature is 295 eV (FWHM) for the 5.9 keV Mn $K\alpha$ line, corresponding to a relative resolution of 5.0%. By lowering the noise level of the preamplifier FET with cryogenic techniques, a resolution of about 200 eV (3.4%) has been achieved (Warburton, Iwanczyk, Dabrowski, Hedman, Penner-Hahn, Roe & Hodgson, 1986).

7.1.6. Position-sensitive detectors (By U. W. Arndt)

Most X-ray diffraction or scattering problems require the quantitative evaluation of a linear or of a two-dimensional pattern. Recent years have seen the development of many different types of linear and area detectors for X-diffraction purposes, that is, of position-sensitive detectors (PSD's) that allow the recording of the positions of the arrival of X-ray photons (Hendricks, 1976; Hendrix, 1982; Arndt, 1986). In addition, imaging detectors have found increasing use in related fields, such as in X-ray astronomy (Allington-Smith & Schwarz, 1984), in X-ray microscopy, in X-ray absorption spectroscopy, and in topography. Here, the emphasis is on the production of an image for direct viewing rather than on the making of quantitative intensity measurements; these applications, in general, require an ultra-high spatial resolution over a relatively small field of view and the ability to cope with very low contrast images: Imaging detectors for topography are discussed in Section 7.1.7. Lessons can also be learnt, and component parts utilized, from quantitative imaging devices developed for visible light.

Progress in these fields has been covered in the *Symposia on Photoelectronic Image Devices* held every 3 years at Imperial College London (since 1960) and in the *Wire Chamber Conferences* (since 1978) and the *London Position-Sensitive Detector Conferences* (since 1987), both reported in full in *Nuclear Instruments and Methods*. Detectors are always one of the principal subjects considered at synchrotron-radiation conferences and workshops, the highlights usually being reported in *Synchrotron Radiation News*. Detectors feature prominently in the proceedings of the *IEEE Symposia on Nuclear Science*, which appear in the *IEEE Transactions*.

Other recent reviews of X-ray detectors are by Fraser (1989), Stanton (1993), Stanton, Phillips, O'Mara, Naday & Westbrook (1993) and Sareen (1994).

The detection of X-ray photons in the energy range of interest for diffraction studies (3 to 20 keV) always involves the interaction of the photon with an inner-shell electron and its complete absorption. The processes that are of interest for the construction of PSD's are of three kinds:

(1) Photography. The characteristics of X-ray film are discussed in Section 7.1.1.

(2) The use of storage phosphors, such as europium-activated barium halide (BaFX:Eu^{2+}, X = Cl or Br) (Sonada, Takano, Miyahara & Kato, 1983; Miyahara, Takahashi, Amemiya, Kamiya & Satow, 1986), which are exposed like photographic film and then scanned with a laser beam causing photon-stimulated light emission of an intensity proportional to the original exciting X-ray intensity; this is measured with a photomultiplier. The plate is re-useable when the X-ray image has been erased. These X-ray detectors have a low background, a large dynamic range, and an adequate spatial resolution. See Section 7.1.8.

(3) Processes that involve the production of electrons. These may be the result of the ionization of a gas; they may be due to the production of electron–hole pairs in a semiconductor; they may be produced in an X-ray photocathode; finally, a phosphor may be used to convert the X-rays into visible light that then produces photoelectrons from a conventional photocathode.

At the present time, X-ray-sensitive photographic emulsions are mainly of historical interest. Storage-phosphor image plates have not only largely replaced photographic film; they have also taken over many of the applications of electronic detectors.

In the following, we are concerned only with detectors that depend on the production of electrons by incident X-rays.

In all detectors, except in semiconductor detectors, the number of primary electrons is multiplied by gas amplification, or in some device such as a microchannel plate or by some other intermediate process. In a PSD, the electron multiplication must take place with a minimum of lateral spread.

Many methods are available for deriving the position of the amplified electron stream or of the cloud of electron–ion pairs (avalanche) in an ionized gas and some of these are discussed below. However, almost any combination of photon detection, electron multiplication, and localization procedure can be used in the construction of PSD's (Fig. 7.1.6.1).

7.1.6.1. *Choice of detector*

Detectors may either be true counters in which individual detected photons are counted or they may be integrating devices that generate a signal that is a function of the rate of arrival of

photons; this signal may then be digitized for recording purposes.

The choice of a linear or of a two-dimensional, or area, PSD depends on its detection efficiency, linearity of response to incident X-ray flux, dynamic range, and spatial resolution, its uniformity of response and spatial distortion, its energy discrimination, suitability for dynamic measurements, its stability, including resistance to radiation damage, and its size and weight.

Before discussing a few of the many types of PSD individually, we shall examine these criteria in a general way. Some of them have been discussed by Gruner & Milch (1982). Table 7.1.6.1 shows the importance, on a scale of 0 to 3, of some of the factors in different fields of study. Other properties, such as stability and sensitivity, are equally important for *all* PSD's.

Table 7.1.6.1. *The importance of some detector properties for different X-ray patterns*

	Type of pattern					
Detector property	Solution	Fibre	Powder	Single crystal	Topographic	Orientation Laue
Spatial resolution	1	2	3	3	3	2
Lack of parallax	0	1	3	3	0	1
Accuracy of intensity measurement	3	3	3	3	1	1
High count rate capability	2	2	2	3	1	1
Suitability for short time slices	3	3	3	2	3	0
Suitability for short wavelengths	0	0	2	2	1	3
Energy discrimination	1	1	2	2	0	0

0 = unimportant; 3 = very important.

7.1.6.1.1. *Detection efficiency*

The detection efficiency of a detector is determined in the first instance by the fraction of the number of incident photons transmitted by any necessary window or inactive layer, multiplied by the fraction usefully absorbed in the active region of the detector. This product, which is often called the absorption efficiency or the quantum efficiency, should be somewhere between 0.5 and 1.0 since the information loss due to incident photons not absorbed in the active region cannot be retrieved by subsequent signal amplification. The *useful* efficiency is best described by the so-called detective quantum efficiency (DQE), ε (Rose, 1946; Jones, 1958). For our purposes, this can be defined as

$$\varepsilon = S^2/\sigma^2 N, \qquad (7.1.6.1)$$

where N is the number of quanta incident upon the detector and σ is the standard deviation of the analogue output signal of amplitude S. For a photon counter with an absorption efficiency q, $S = qN$, $\sigma = (qN)^{1/2}$, and $\varepsilon = q$. An analogue detector with a DQE ε thus behaves like a perfect counter that only detects a fraction ε of the incident photons.

Under favourable conditions, the DQE of analogue detectors for X-rays is in excess of 0.5, but ε varies with counting rate and is lower for detectors with a very large dynamic range, as shown below.

The DQE of CCD- and vidicon-based X-ray detectors has been discussed by Stanton, Phillips, Li & Kalata (1992*a*).

7.1.6.1.2. *Linearity of response*

The linearity of a counter depends on the counting losses, which are due to the finite dead-time of the counter and its

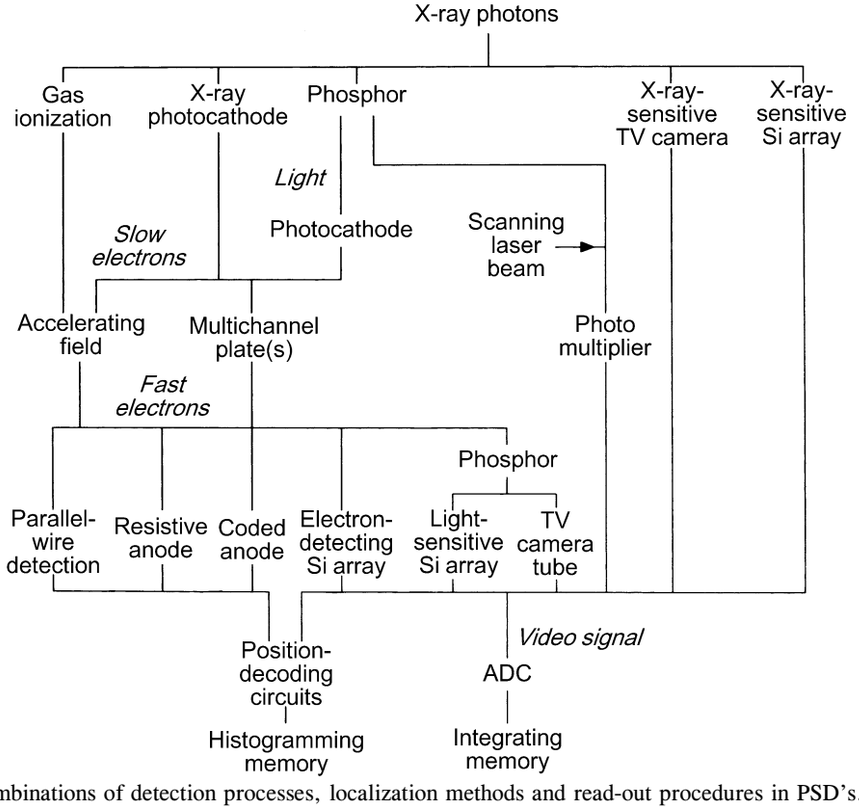

Fig. 7.1.6.1. Possible combinations of detection processes, localization methods and read-out procedures in PSD's.

processing circuits. The counting losses are affected by the time modulation, if any, of the source, as, for example, with storage rings (Arndt, 1978).

Counting losses can affect the behaviour of detectors in two different ways. In most analogue detectors and in counters with parallel read-out, each pixel behaves as an independent detector and the counting loss at any point depends only on the *local* counting rate. In other devices, such as multiwire proportional chambers with delay-line read-out (see Subsection 7.1.6.2), the whole detector becomes dead after an event anywhere in the detector and what matters is the *global* counting rate.

Fortunately, the fractional counting loss is the same for all parts of the pattern so that the *relative* intensities in a stationary pattern are not affected.

7.1.6.1.3. *Dynamic range*

The lowest practically measurable intensity is determined by the inherent background or noise of the detector. Some form of discrimination against noise pulses is usually possible with a detector that counts individual photons, but not, of course, with integrating detectors.

The maximum intensity at which a *counter* can operate is determined by the dead-time. In the case of an *integrating or analogue detector* with a variable gain, there is a trade-off between maximum intensity and DQE. Such a device can often be regarded as having an output signal with an amplitude $S = NV/M$ that is a noise-free representation of N, the number of photons detected in the integrating period of the device, where V, the maximum signal amplitude, is produced by M photons in this period. M can be varied by altering the gain of the detector. The noise can be regarded as a fixed fraction $1/r$ of the maximum amplitude V that is added to the signal. Then the DQE will be

$$\begin{aligned}\varepsilon &= S^2/\sigma^2 N \\ &= (1 + M^2/r^2 N)^{-1}. \qquad (7.1.6.2)\end{aligned}$$

This equation shows the importance of having as small a value of $1/r$ as possible; it also demonstrates that, for a given value of r, M can be increased only at the expense of a reduced DQE. This is valid for X-ray film (Arndt, Gilmore & Wonacott, 1977), for television detectors (Arndt, 1984), for the integrating gas detectors discussed in Subsection 7.1.6.2, and for many semiconductor X-ray detectors.

7.1.6.1.4. *Spatial resolution*

The spatial resolution of a PSD is determined by the number and size of resolution or picture elements (pixels) along the length or parallel to the edge of the detector. In most diffraction experiments, the size of the pattern can be scaled by altering the distance of the detector from the sample and what is important is the angular resolution of the detector when placed at a distance where it can 'see' the entire pattern. We shall see below that linear PSD's can be made with up to 2000 pixels and that area detectors are mostly limited to fewer than 512×512 pixels. The sizes of pixels range from about 10 μm for semiconductor PSD's to about 1 mm for most gas-filled detectors.

The *useful* number of pixels of a detector is determined by its point-spread function (PSF). This is the relative response as a function of distance from the centre of a point image on the detector. PSF's are not necessarily radially symmetrical and may have to be specified in at least two directions at right angles, for example along and perpendicular to the lines of a television raster scan. The width of the PSF at the 50% level determines the amount of detail visible in a directly viewed image. The accuracy of intensity measurements may depend more critically upon the width of the PSF at a lower level, since a weak spot may be immeasurable when sitting on the 'tail' of a very intense one. For various physical reasons, the PSF's of *all* PSD's, including X-ray film, have appreciable tails.

The spatial resolution of a detector is affected by parallax: when an X-ray beam is absorbed in a thick planar detector at an angle φ to the normal, the width of the resultant image is smeared out exponentially and its centroid is shifted by an amount $\sin\varphi/\mu$. For 8 keV X-rays incident at 45° on a xenon-filled counter, for example, this shift is about 4 mm for a filling pressure of 1 atm and 0.4 mm for a filling pressure of 10 atm. These figures illustrate the desirability of high-pressure xenon (Fig. 7.1.6.2) for gas-ionization detectors intended for wide-angle diffraction patterns.

7.1.6.1.5. *Uniformity of response*

All PSD's show long-range and pixel-to-pixel variations of response to larger or smaller extents. These can be corrected, in general by means of a look-up table, during data processing, but the measurements necessary for the calibration are often time-consuming. The output signals of many analogue detectors contain fixed-pattern noise that is synchronous with the read-out clock. This noise is usually removed during data processing, which in any case requires the subtraction of the background pattern.

7.1.6.1.6. *Spatial distortion*

In most detectors, there is some spatial distortion of the image. Again, the necessary calibration procedure may be time-consuming. Distortions cause point-to-point variations in pixel size, which produce response variations additional to those from other causes.

Corrections for spatial distortion and for non-uniformity of response have been discussed by Thomas (1989, 1990) and by Stanton, Phillips, Li & Kalata (1992*b*).

7.1.6.1.7. *Energy discrimination*

The amplitude of the signal due to a single photon is usually a function of the photon energy. The variance in this amplitude, or the full width at half-maximum (FWHM) of the pulse-height spectrum, for a monoenergetic input, depends on the statistics of the detection process. A sharp pulse-height-distribution (PHD) curve may permit simultaneous multi-wavelength measurements with a suitable counter, or at least afford a reduction of the background by pulse-height discrimination. In an analogue

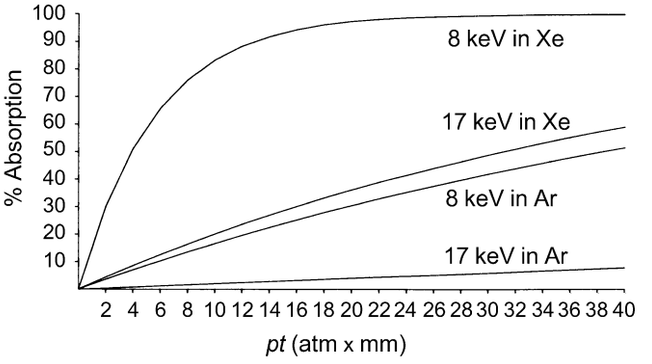

Fig. 7.1.6.2. Absorption of 8 keV and 17 keV photons in argon and xenon as a function of pressure in atm × column length in mm.

detector, the variance in the primary amplitude affects the DQE (Arndt & Gilmore, 1979).

7.1.6.1.8. *Suitability for dynamic measurements*

Many investigations, such as low-angle or fibre diffraction studies on biological materials carried out with synchrotron radiation (Boulin, Dainton, Dorrington, Elsner, Gabriel, Bordas & Koch, 1982; Huxley & Faruqi, 1983), involve the time variation of a diffraction pattern. For very short time slots, only counters can be employed; the incoming pulses must then be gated and stored in an appropriate memory (Faruqi & Bond, 1982).

Stores used for these experiments are described as histogramming memories; the contents of a given storage location are incremented by one whenever the corresponding address, which represents the position and the time of arrival of a photon, appears on the address bus (Hendricks, Seeger, Scheer & Suehiro, 1982; Hughes & Sumner, 1981).

7.1.6.1.9. *Stability*

Stability of the performance of a detector is of paramount importance. Most position-sensitive detectors are used in connection with microcomputers, which make calibration and corrections for spatial distortion, non-uniformity of response, and lack of linearity relatively easy, provided that these distortions remain constant. The long-term stability of many detectors, notably of semiconductor devices, is affected by radiation damage produced by prolonged exposure to intense irradiation.

7.1.6.1.10. *Size and weight*

The size and weight of the detector determine the ease with which the detector can be moved relative to the sample and thus the extent to which the diffractometer can be adapted to varying resolution and collimation conditions. Some detectors cannot be moved easily (Xuong, Freer, Hamlin, Nielsen & Vernon, 1978), or need very heavily engineered rotational and translational displacement devices (Phizackerley, Cork & Merritt, 1986). Others, such as spherical drift chamber multiwire proportional chambers, are designed for use at a fixed distance from the sample and may only be swung about the latter but not translated (Kahn, Fourme, Bosshard, Caudron, Santiard & Charpak, 1982).

In single-crystal diffraction patterns, the Bragg reflections may be visualized as diverging from the X-ray source while the background – fluorescence X-rays, scatter by amorphous material on the specimen crystal and its mount – diverges from the sample. Consequently, the highest reflection-to-background ratio is achieved by using a large detector at a large distance from the specimen. Of all the detectors discussed here, the image plate can most readily and economically be used to cover a large area; its present popularity is chiefly due to this property (Sakabe, 1991).

There is fairly general agreement on the specification of an ideal X-ray area detector. It should be at least 250 mm in diameter, contain at least 1000×1000 pixels, have a large dynamic range and a high detective quantum efficiency for photon energies up to 20 keV and be capable of being read-out rapidly.

Many suggestions have been made for improving the performance of existing detectors. It has become apparent, however, that the development of ideal, or even better, X-ray detectors is extremely expensive and, therefore, that their development and installation can be undertaken only in central national or international laboratories such as storage-ring synchrotron-radiation laboratories.

7.1.6.2. *Gas-filled counters*

In all gas-filled counters, whether one-, two-, or three-dimensional, the initial event is the absorption of the incoming X-ray photon in a gas molecule with the emission of a photo-, or alternatively an Auger, electron. The detection efficiency depends on the fraction of the photons absorbed in the gas and this fraction is shown in Fig. 7.1.6.2 as a function of the product of gas pressure and column length for 8 and 17 keV photons on argon and xenon. The ionization energy of noble gases is about 30 eV so that one 8 keV photon gives rise to about 270 electron–ion pairs. With adequately high collecting fields, the electrons acquire sufficient energy to produce further ionization by collision with neutral filling gas molecules; this process is often referred to as 'avalanche production' or 'gas multiplication'. The factor A by which the number of primary ion pairs is multiplied can be as great as ten to one hundred thousand. Up to a certain value of A, the total amount of ionization remains proportional to the energy of the original X-ray photon. The electrical signal generated at the anode of the counter is due very largely to the movement of the positive ions from the immediate vicinity of that electrode; at the same time, a corresponding pulse is induced on the cathode. The signal can be shaped to produce a pulse with a duration of the order of a microsecond.

In single or multiwire proportional counters, the secondary ionization (avalanche production) takes place in the highest field region, that is, within a distance of a few wire diameters of the anode wire or wires. The electrons are collected on the anode and the positive ions move towards the cathode, with very little spread of the ionization in a direction perpendicular to the field gradient, that is, parallel to the wire direction. It is thus possible to construct position-sensitive devices based on such chambers.

Proportional-counter behaviour is discussed in detail in many standard texts and review articles (Wilkinson, 1950; Price, 1964; Dyson, 1973; Rice-Evans, 1974).

The gas amplification does not have to take place in the same region of the detector as the original absorption. In so-called drift chambers, the primary ionizing event takes place in a low-field region where no avalanching takes place. The electrons drift through a grid or grids into a region where the field is sufficiently high for gas multiplication to occur. The drift field can be made cylindrical in a linear counter (Pernot, Kahn, Fourme, Leboucher, Million, Santiard & Charpak, 1982), or spherical in an area detector (Charpark, 1982; Kahn, Fourme, Bosshard, Caudron, Santiard & Charpak, 1982), centred on the point from which the X-rays diverge, that is on the specimen; the electrons then drift in a radial direction without parallax being introduced (Fig. 7.1.6.3).

In many experiments, use is made of the energy discrimination of the detector. The ratio of the full width at half-maximum to the position of the maximum of the pulse-height distribution is given by

$$w = 2.36[(F + f)/N], \qquad (7.1.6.3)$$

where N is the number of primary ion pairs produced, F is the Fano factor (Fano, 1946, 1947), which takes into account the partially stoichastic character of the gas multiplication process, and f is the avalanche factor. For proportional counters filled with typical gas mixtures (argon + methane), $F = 0.17$ and $f = 0.65$, so that for 8 keV photons $w \sim 13\%$, but, in the

so-called Penning gas mixtures (*e.g.* noble gas and ethylene), f can approach zero at a certain field strength. In a wire counter with its rapidly varying field strength, f is small only for a gas amplification of less than 50. The energy resolution for 8 keV photons could then be as low as 6%, but the pulses induced on the cathode wires of a MWPC are then too small to permit a precise localization. This problem has been overcome by using uniform-field avalanching in two regions in tandem, separated by a drift space (Schwarz & Mason, 1984, 1985). The energy information was derived after the first low-gain gas multiplication process ($A \sim 500$): a proportion of the electrons from the first avalanche then drifted into the second avalanche region which boosted the gas gain to more than 10^5, necessary to give a high spatial resolution.

In an alternative method (Charpak, 1982; Siegmund, Culhane, Mason & Sanford, 1982), the additive avalanche factor f is eliminated by deriving the energy information, not from the collected charge, but from the visible light pulse produced by the individual avalanches of each primary electron.

7.1.6.2.1. *Localization of the detected photon*

There are several methods of deriving the position of the detected photon that are applicable to both linear and area detectors.

(1) The charge produced in the avalanche can be collected on a resistive anode. In the case of linear detectors, the central wire can be given a low or a very high resistance. The latter type is most commonly made from a quartz fibre coated with carbon. The emerging pulse is detected at both ends of the wire (Borkowski & Kopp, 1968; Gabriel & Dupont, 1972). Area detectors with a resistive disc anode must have at least three read-out electrodes (Stümpel, Sanford & Goddard, 1973). With low-resistance electrodes, the position of the event can be computed by analogue circuits from the relative pulse amplitudes (Fig. 7.1.6.4*a*); a preferred method with high-resistance anodes is to measure the rise times of the output pulses that are determined by the time constant formed by the input capacity of the pulse amplifier at each output and the resistance of the path from the detection point to the output electrode (Fig. 7.1.6.4*b*).

(2) The anode or cathode can be constructed in the form of two or more interleaved resistive electrodes insulated from each other. Provided that the charge distribution covers at least one unit of the pattern, positional information can be derived by relative pulse height or by timing methods. Examples of this type of read-out are the linear backgammon (*jeu de jacquet*) counter together with its two-dimensional variant (Allemand & Thomas, 1976), the wedge-and-strip anode developed by Anger and his collaborators (Anger, 1966; Martin, Jelinsky, Lampton, Malina & Anger, 1981), and its polar coordinate analogue (Knibbeler, Hellings, Maaskamp, Ottewanger & Brongersma, 1987), for two-dimensional read-out. The method seems capable of a higher spatial resolution than any other (Schwarz & Lapington, 1985).

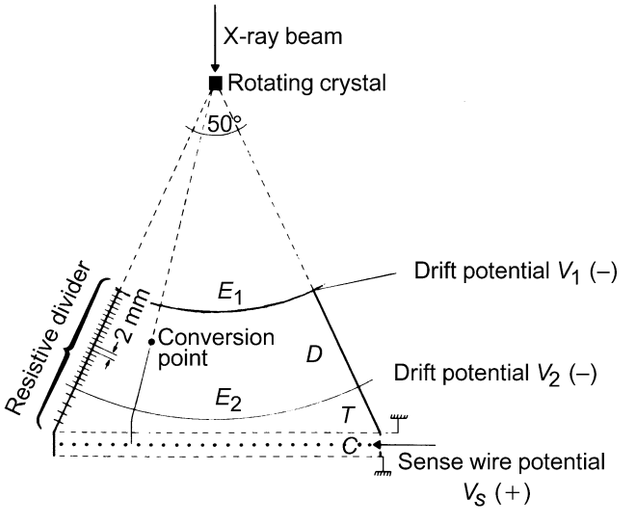

Fig. 7.1.6.3. Spherical drift chamber multiwire proportional chamber (MWPC) (Charpak, 1982; courtesy of G. Charpak).

(3) The anode or cathode can be made from a number of sections connected to a tapped delay line (Fig. 7.1.6.4*c*). Positional information is derived from the time delay of the pulse relative to the arrival of an undelayed prompt pulse. Linear PSD's (LPSD's) with delay-line read out are usually made straight, but variants have been produced in the form of circular arcs (Wölfel, 1983; Ballon, Comparat & Pouxe, 1983).

Area detectors of this type require two parallel planes of parallel wires with the wires in the two planes at right angles to one another placed on either side of the anode, which also consists of parallel wires. The prompt pulse in such a detector, the multiwire proportional chamber (MWPC), is usually taken from the anode (Fig. 7.1.6.5). In counters without a drift space, the electron avalanche always ends up on one anode wire, and there is then a pseudo-quantization in the position measurement made at right angles to the direction of the anode wires. In drift-space detectors with a narrow anode-wire spacing, the avalanche lands on more than one wire and some interpolation is possible. In the direction parallel to the anode wires, there is never any quantization and the resolution can be better than the cathode wire spacing: Although pulses are induced on several wires, the centroid of the delayed group of pulses can be measured with precision. Delay-line read-out LPSD's have reached the highest resolution in the hands of Radeka and his group (Smith, 1984). MWPC's of this type have been used for several years (Xuong, Freer, Hamlin, Nielsen & Vernon, 1978; Bordas, Koch, Clout, Dorrington, Boulin & Gabriel, 1980; Baru, Proviz, Savinov Sidorov, Khabakhshev, Shuvalov & Yakovlev, 1978; Anisimov, Zanevskii, Ivanov, Morchan, Peshekhonov, Chan Dyk Tkhan, Chan Khyo Dao, Cheremukhina & Chernenko, 1986). They have a relatively low maximum count rate ($< 10^5$ s^{-1}) determined by the space charge due to earlier events and by the fact that position digitization takes of the order 1 μs. Limitations in the closeness of practicable wire spacing leads to a pixel size of the order of 1 mm.

(4) A faster read out is possible with MWPC's in which the positional information is derived from the centroid in amplitude of the group of induced cathode pulses (Fig. 7.1.6.4*d*). Individual amplifiers of carefully equalized gain are required for each individual wire or at least for small groups of adjacent wires (Pernot, Kahn, Fourme, Leboucher, Million, Santiard & Charpak, 1982). Counting rates in excess of 10^6 s^{-1} are then possible.

7.1.6.2.2. *Parallel-plate counters*

In the gas-filled detectors that we have considered so far, the electric field is cylindrically symmetrical in the immediate vicinity of the wire or wires near which gas multiplication takes place and the maximum count rate is limited ultimately by the electrostatic shielding effect of the ion sheath owing to previous X-ray photons. In parallel-plate chambers, the electrodes are in the form of very fine electro-formed grids: With this structure, the pulse shape is quite different; the very sharp initial part, due to the rapidly moving electrons, can be separated, at the expense

of a loss of signal amplitude, from the slow component due to the positive ions; in addition, the shielding effect is much less pronounced. Accordingly, counting rates up to at least $10^{11}\,s^{-1}\,m^{-2}$ are possible with parallel-plate PSD's (Stümpel, Sanford & Goddard, 1973; Peisert, 1982; Hendrix, 1984).

7.1.6.2.3. *Current ionization PSD's*

For the very highest counting rates, it is necessary to abandon all methods in which individual X-ray photons are counted and instead to measure the ionization current produced by the incident X-rays on either cathode or anode. Fig. 7.1.6.6 shows the principles of a cathode read-out linear PSD. The cathode is divided into strips, each of which is connected to a capacitor and to an input terminal of a CMOS analogue multiplexer. The charge accumulated on each capacitor in a given time period is transferred to a charge-sensitive amplifier when the associated channel is selected by an addressing signal. The output voltage of the amplifier is digitized by means of an analogue-to-digital converter. The complete pattern is scanned by incrementing the addresses sequentially: The resolution is that of the strip spacing (~0.5 mm) and the principle can be extended to two dimensions (Hasegawa, Mochiki & Sekiguchi, 1981; Mochiki, Hasagawa, Sekiguchi & Yoshioka, 1981; Mochiki, 1984; Mochiki & Hasegawa, 1985). Global count rates in excess of $10^9\,s^{-1}$ are possible with this method. Lewis (1994) has published a

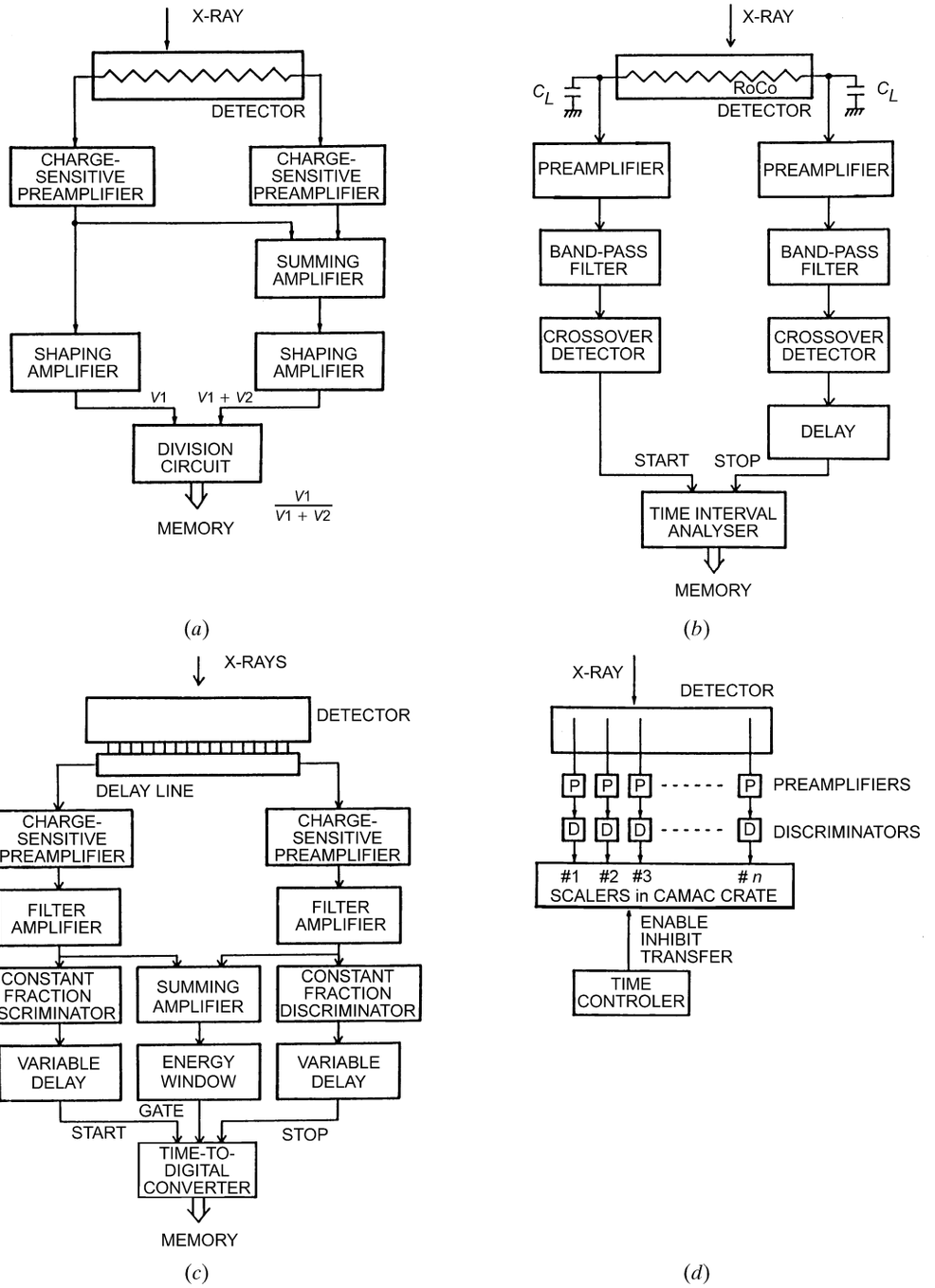

Fig. 7.1.6.4. Read-out methods for gas-filled LPSD's. (*a*) Charge division with low-resistance anode wire. (*b*) Rise-time method with high-resistance anode. (*c*) Delay-line read-out. (*d*) Amplifier-per-wire method. From Mochiki (1984); courtesy of K. Mochiki.

comprehensive survey of the present status and the future potentialities of gas-filled position-sensitive detectors.

7.1.6.3. *Semiconductor detectors*

Semiconductor detectors are essentially solid-state ionization chambers in which the incoming photon generates electron–hole pairs instead of electron–ion pairs. Semiconductor detectors are sensitive to the entire electromagnetic spectrum from visible to X-rays, and they can also detect electrons directly. There are, therefore, three possible methods of constructing semiconductor X-ray detectors, each of which has its advantages and disadvantages.

(1) They can be exposed directly to the incoming X-rays.

(2) The X-ray photons can be made to produce visible light photons that are then detected in a light sensor.

(3) The X-rays can be made to produce electrons that are detected by the semiconductor detector.

In semiconductor one- or two-dimensional PSD's, the detector and the read-out circuitry are usually integrated on the same chip. In these devices, the pixel size and position are fixed once and for all so that they are geometrically completely stable. Integrated read-out circuitry has a low input capacity and thus an extremely low read-out noise.

All semiconductor X-ray PSD's are derived from imagers for visible light, which are of two basic types: photodiode arrays (PDA's) and charge-coupled devices (CCD's) (Lowrance, 1979; Allinson, 1982; Borso, 1982; Third European Symposium on Semiconductor Detectors, 1984).

In PDA's, the detection of a photon-generated charge takes place in a depletion layer that is formed either in a suitably biased *p–n* diode or in a metal-oxide-semiconductor (MOS) capacitor. The electron–hole pairs are separated by the field associated with the depletion layer. The individual diodes store charge during the integration period; this is read out into a common video output line *via* MOS multiplexing switches. This architecture is usually adopted for linear arrays where the switches can be arranged around the periphery of the diodes with a minimum amount of dead space between them and where they can be shielded from the incident X-rays. PDA's tend to suffer from a high fixed-pattern noise due to differences in the performance of individual MOS switches.

In CCD's (Howes & Morgan, 1979), the sensing elements are always MOS capacitors suitably biased to establish charge-storage volumes. During read out, the charge is transferred in a 'bucket-brigade' fashion from one MOS capacitor to the next until it reaches the output. In linear CCD's, this output is at one end of what is essentially an analogue shift register. Most two-dimensional CCD's are frame-transfer devices: at the end of the exposure, the charge is transferred line by line to an identical array of MOS elements; while the next 'frame' is exposed in the image array, the contents of the buffer array are transferred, one line at a time, to a single-line buffer from which they are shifted out element by element. Since the transfer circuitry in CCD's is interlaced with the detector elements, they are more difficult to shield and are more subject to radiation damage.

7.1.6.3.1. *X-ray-sensitive semiconductor PSD's*

For X-ray diffraction applications, the main disadvantage of semiconductor devices is that the universal trend in their manufacture is in the direction of miniaturization, leading to a very small pixel size. Thus, imaging devices with up to 2000×2000 pixels have been produced but the pixel size is typically $\sim 10\,\mu m$ for CCD's and $\sim 20\,\mu m$ for PDA's; in most X-ray diffraction applications, it would be difficult to scale down sample and source sizes to a point where the pattern size is

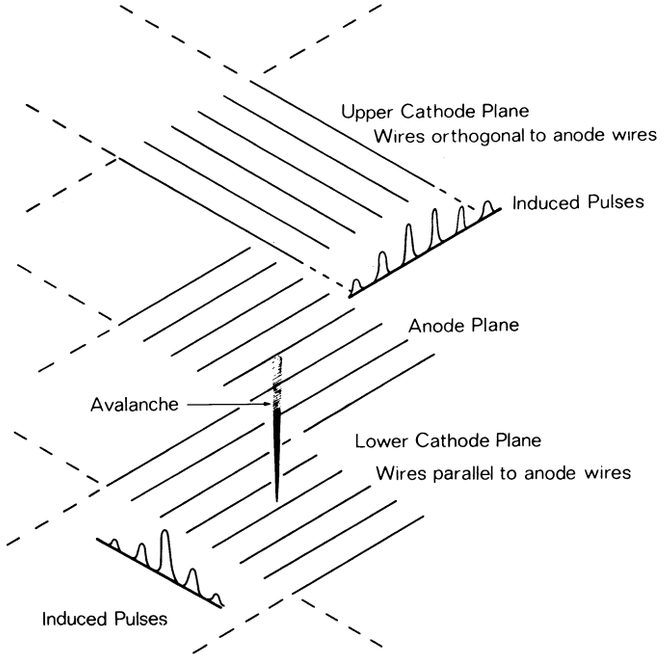

Fig. 7.1.6.5. Three-plane MWPC. Note the pseudo-quantization due to charge collection on one anode wire. The cathode wires may either be connected to a tapped delay line as in Fig. 7.1.6.4(*c*) or to individual amplifiers as in Fig. 7.1.6.4(*d*) (courtesy of A. R. Faruqi).

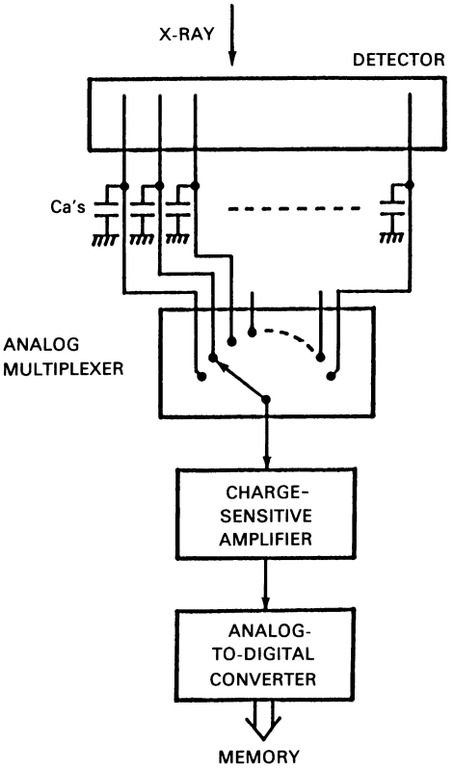

Fig. 7.1.6.6. Integrating LPSD. From Mochiki (1984); courtesy of K. Mochiki.

appropriate to a semiconductor imager, even though a 2000×2000 CCD with $27 \times 27\,\mu m$ pixels is available.

Semiconductor point counters cooled to 80 K are characterized by their very high energy resolution (better than 2% in the 8 keV region). Some counting PSD's potentially have a similar energy resolution. Two-dimensional X-ray-sensitive CCD's for X-ray astronomy research have been used as photon counters (Walton, Stern, Catura & Culhane, 1985; Lumb, Chowanietz & Wells, 1985) but they can only be used at very low counting rates. In integrating devices, the energy discrimination is lost. Silicon detectors for visible-light applications are made with depletion depths of the order of 10 μm. For the detection of 8 keV photons with more than 90% efficiency, depletion depths of 165 μm are necessary and these can be produced only from very high resistivity material (Howes & Morgan, 1979). Moreover, in commercial visible-light imagers, the depletion region is covered by circuitry or by an inactive layer that constitutes an absorbing window for X-ray detection. For the detection of X-rays or electrons, it is, therefore, customary to thin the device and to illuminate it from the back (see, for example, Meyer-Ilse, Wilhelm & Guttmann, 1993).

One-dimensional X-ray detectors utilizing PDA's, such as those made by the Reticon Corporation, have found a number of applications, especially in dispersive X-ray absorption spectroscopy (EXAFS) (Jucha, Bonin, Dartyge, Flank, Fontaine & Raoux, 1984).

A particular problem with silicon detectors is the damage caused by the incidence of X-rays or of energetic electrons. The effects can be minimized by masking all but the active part of their device and by operating it at low temperatures (Jucha *et al.*, 1984).

The use of the room-temperature semiconductor mercuric iodide in place of silicon seems promising (Patt, Delduca, Dolin & Ortale, 1986).

The X-ray diffraction applications of directly sensitive semiconductor PSD's are likely to remain limited. A previous conversion to visible light or to electrons offers the possibility of an optical or electron-optical demagnification onto the imager, as well as of avoiding some of the other problems discussed above (Deckman & Gruner, 1986).

7.1.6.3.2. *Light-sensitive semiconductor PSD's*

Standard light-sensitive semiconductor imaging devices can be used for X-ray detection if the X-rays are first converted to light by means of a phosphor. One 8 keV X-ray photon produces several hundred light photons in a good phosphor (see Table 7.1.6.2). Because of the low noise levels possible with cooled CCD's (~10 electrons r.m.s.), only 1 to 3% of these photons need to reach the device to produce a perfect X-ray detector. Unfortunately, even this is possible only with optics that do not demagnify to any considerable extent (see Subsection 7.1.6.5) and one is thus restricted to a small detector. However, CCDs are now available that can be butted along two or three edges and these make possible the construction of 'tiled' detectors that contain four or six of such CCD chips (Burke, Mountain, Harrison, Bautz, Doty, Ricker & Daniels, 1991; Fordham, Bellis, Bone & Norton, 1991; Allinson, 1994). Individual channels can be read simultaneously (Hopf & Rodricks, 1994), thus making possible a relatively rapid read out of a large number of pixels.

7.1.6.3.3. *Electron-sensitive PSD's*

In image intensifiers, an output image is produced on a phosphor screen by electrons with an energy of a few keV. A promising device with direct positional read out consists of a demagnifying intensifier in which the phosphor is replaced by a CCD. Various intensifiers have been described in which the electrons reaching the CCD have an energy of several keV so that the electron–hole generation is amplified (EBS process) (Lowrance, Zucchino, Renda & Long, 1979; Lemonnier, Richard, Piaget, Petit & Vittot, 1985). High-energy electrons are liable to cause radiation damage and similar precautions as for X-rays, such as thinning and back-illumination, are necessary. Experiments have been reported with less-damaging low-energy (200 eV) electrons produced in a microchannel plate (MCP) image intensifier (Dereniak, Roehrig, Salcido, Pommerrenig, Simms & Abrahams, 1985). Both approaches look promising but it is questionable whether a device with an X-ray phosphor input and of adequate size and resolution at an affordable price will emerge in the near future.

7.1.6.4. *Devices with an X-ray-sensitive photocathode*

Image converters and television cameras with X-ray-sensitive photocathodes have been reported. These cathodes must be thin, or they must have a low bulk density to allow the photoelectrons to escape (Bateman & Apsimon, 1979; Haubold, 1984).

Television tubes with a beryllium window and a 25 mm diameter lead oxide target are available and experimental 125 mm tubes have been described (Suzuki, Uchiyama & Ito, 1976).

X-ray-sensitive Saticon television camera tubes with an amorphous selenium–arsenic target (Chikawa, Sato & Fujimoto, 1984) have an active diameter of only 10 mm but a limiting resolution (MTF = 5%) of 6 μm. They have an absorption efficiency of 52% for Mo $K\alpha$ radiation and are used mainly for X-ray topography. Other X-ray-sensitive television camera tubes have been described by Matsushima, Koyama, Tanimoto & Tano (1987), Suzuki, Hayakawa, Usami, Hirano, Endoh & Okamura (1989) and Sato, Maruyama, Goto, Fujimoto, Shidara, Kawamura, Hirai, Sakai & Chikawa (1993). Such tubes are discussed further in Section 7.1.7.

7.1.6.5. *Television area detectors with external phosphor*

Much development has gone into quantitative measurements with area detectors in which the diffraction pattern is formed on an external phosphor fibre-optically coupled to a low-light-level television camera. Mostly the television camera embodies a demagnifying image intensifier coupled *via* demagnifying optics to a sensitive television camera tube (Arndt & Gilmore, 1979; Arndt, 1982; 1985; Arndt & In't Veld, 1988; Kalata, 1982, 1985; Gruner, Milch & Reynolds, 1982) or to a CCD or an array of CCD's (Strauss, Naday, Sherman, Kraimer & Westbrook, 1987; Strauss, Westbrook, Naday, Coleman, Westbrook, Travis, Sweet, Pflugrath & Stanton, 1990; Templer, Gruner & Eikenberry, 1988; Widom & Feng, 1989; Fuchs, Wu & Chu, 1990; Karellas, Liu, Harris & D'Orsi, 1992). Camera tubes were frequently read at commercial television rates (625 lines with a field repetition rate of 25 Hz or 525 lines with a field repetition rate of 30 Hz in Europe and in North America and Japan, respectively), leading to pixel rates of about 10 MHz. Successive images were then digitized and their sums stored in memory (see Fig. 7.1.6.7). Milch, Gruner & Reynolds (1982) developed a slow-scan method for a silicon-intensifier-target (SIT) tube. This latter method has been facilitated by the development of very large scale integration memory circuits, which have made it possible to construct economical image stores into which the camera can write at a slow rate and which can then be read at normal television rates for display purposes.

Table 7.1.6.2. *X-ray phosphors (from Arndt, 1982)*

Phosphor	Type	Bulk density	No. of photons per 8 keV quantum		Max. emission wavelength (nm)	Decay to 1% (s)
			Produced	Collected*		
ZnS (Ag)	Polycrystal	4.1	750	300	450	3×10^{-7} + slow components
Gd_2O_2S	Polycrystal	7.1	500	200	550	10^{-3}
CsI (Tl)	Monocrytal	4.5	240	62	580	10^{-6}

* These figures are for collection on a photocathode on the opposite side of a fibre-optics face plate, in the absence of a reflective coating.

CCD's are usually operated in this fashion, so that the read–out circuits can have a narrow band-width and produce an excellent signal-to-noise ratio.

For very low X-ray intensities in which the probability of the arrival of a photon per pixel per frame period is much less than one, the camera can be operated at normal frame frequencies in a digital mode. Specially designed circuits detect the charge image produced by a single X-ray photon and find the centroid of this image (Kalata, 1982); the events are 'counted' in a histogramming memory. The method is capable of some energy discrimination and has a high spatial resolution because the centroid of the image can be found to a high precision.

7.1.6.5.1. *X-ray phosphors*

The incoming X-rays are converted to light in a phosphor that is coupled to the first photocathode of the system. Both polycrystalline and monocrystalline phosphors are used for X-ray detection. The former give a higher light output but have a limited resolution; the latter tend to have a poorer light-conversion efficiency but have the best resolution. The most useful phosphors are shown in Table 7.1.6.2.

Many attempts have been made to improve the spatial resolution of phosphor screens by constructing them in the form of scintillating fibres that are optically isolated from one another so that the scintillation does not spread. This can be achieved by growing columnar scintillating crystals (Oba, Ito, Yamaguchi & Tanaka, 1988), by intagliating polycrystalline phosphors (Fouassier, Duchenois, Dietz, Guillemet & Lemonnier, 1988) and by using arrays of scintillating fibres (Bigler, Polack & Lowenthal, 1986; Ikhlef & Skowronek, 1993, 1994).

Image intensifiers designed for radiography with relatively hard radiation usually have an X-ray-transparent window – which may be up to 300 mm in diameter – and an *internal* phosphor–photocathode sandwich deposited on an X-ray-transparent substrate. Problems of compatibility of phosphor and photocathode have restricted the phosphor used, but CsI works well with multialkali photocathodes. Moy and his collaborators have constructed a large-diameter television detector in which the image intensifier has been modified by using beryllium for the window and for the sandwich substrate; this intensifier is coupled to a slow-scan CCD camera (Moy, 1994).

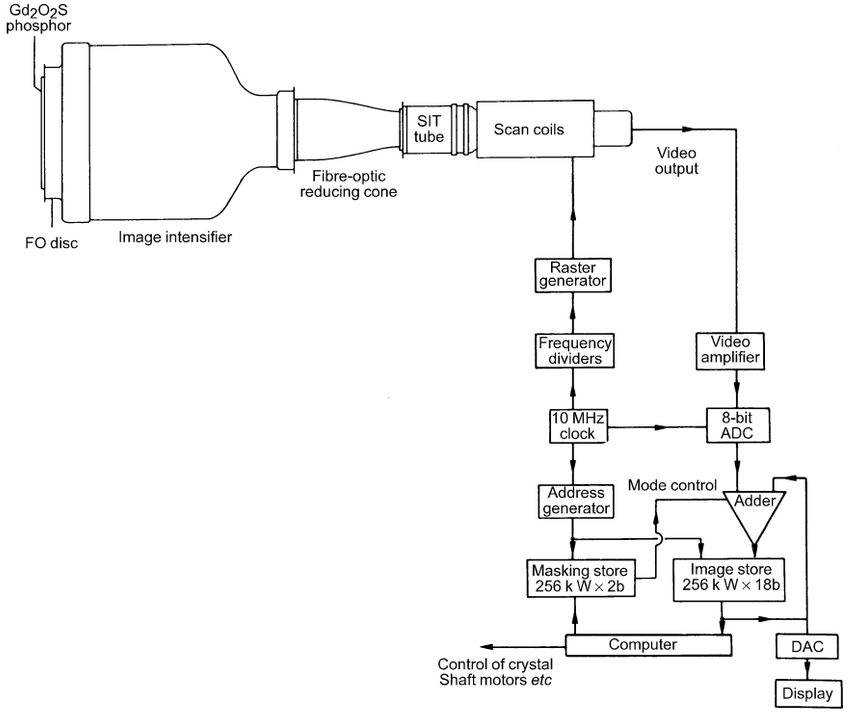

Fig. 7.1.6.7. Fast-scanning television X-ray detector (after Arndt, 1985).

7.1.6.5.2. *Light coupling*

Each incident X-ray photon should give rise to several photoelectrons from the first photocathode in order to achieve a high DQE (Arndt & Gilmore, 1979). The best photocathodes have a yield of about 0.2 electrons per light photon; only fibre-optics coupling between the phosphor and the photo-cathode can give an adequate light-collection efficiency (in excess of 80% for 1:1 imaging). With demagnifying fibre optics, the light loss is considerable for purely geometrical reasons. Fibre-optic cones, in which each individual glass fibre is conical, are available for magnification or demagnification up to about 5:1. It should be noted that image intensifiers and TV tubes with electrostatic focusing are normally made with fibre-optics face-plates and that some CCD's are also available with fibre-optics windows.

Where lens optics must be employed, it is best to use two infinity-corrected objectives of the same diameter, but not necessarily of the same focal length, back to back. In practice, the best light-collection efficiency that can be achieved at a demagnification of M is about $(2M)^{-2}$. It is for this reason that there are limitations on the maximum size of image that can be projected onto a CCD without the use of an image intensifier (but see Naday, Westbrook, Westbrook, Travis, Stanton, Phillips, O'Mara & Xie, 1994; Koch, 1994; Allinson, 1994). The function of this intensifier is to match a relatively large diameter X-ray phosphor to a small-size read-out device. As a result of the high sensitivity of CCD's, especially of slow-scan CCD's, a low photon gain in the intensifier and a low light-coupling efficiency in the coupling between intensifier and read-out device are quite adequate. It is, however, essential to couple the X-ray phosphor as efficiently as possible to the photocathode.

Roehrig *et al.* (1989) have described a design in which an image intensifier with 150 mm diameter input and output face plates is coupled by means of six demagnifying fibre-optic cones to six CCD's. Allinson (1994) has examined the need for image intensification and has shown that it is possible to construct a 150 mm square detector that has a performance approaching that of an ideal detector without using an image intensifier. Different methods of light coupling and format alteration have been discussed by Deckman & Gruner (1986).

7.1.6.5.3. *Image intensifiers*

In an image intensifier, the photoelectrons from a photocathode are made to produce a visible intensified image on an output phosphor. In so-called first-generation tubes, the intensification is produced by subjecting the electrons to accelerating voltages of up to about 15 keV: the number of visible-light photons at the output per keV of electron energy is about 80. The photon gain of the devices is typically about 100; there may be a brightness gain factor of M^2 if the electrostatic electron-optical system produces a demagnification of M. Standard first-generation image intensifiers of this type are made with input field diameters up to 80 mm, they always have fibre-optics input face plates on which X-ray phosphor may be deposited, they are stable and robust, and have a good resolution of better than 100 μm at the input. Their low gain requires the use of a low-light-level TV camera tube in the next stage (Arndt & Gilmore, 1979) or of two or more intensifiers of this type in tandem (Kalata, 1982) or of an intrinsically more sensitive slow-scan read out (Eikenberry, Gruner & Lowrance, 1986).

For military and civilian night-vision applications, first-generation image intensifiers have largely been replaced by devices embodying one or two microchannel plates (MCP's) that produce an electron gain of up to 1000 per stage (see, for example, Emberson & Holmshaw, 1972; Garfield, Wilson, Goodson & Butler, 1976). Commercial second- and third-generation intensifiers (Pollehn, 1985) are less suitable for quantitative scientific purposes than the first-generation devices: their GaAs photocathodes are less well matched to most X-ray phosphors, the gain of MCP's decreases with time, and the tubes have a slightly lower resolution than diode types of comparable diameter. Most third-generation intensifiers have plain rather than fibre-optics face plates and none appear to be available with a diameter greater than 50 mm (Airey & Morgan, 1985). Nevertheless, these high-gain intensifiers do make it possible to construct relatively cheap moderate-performance X-ray detectors using standard-sensitivity TV pick-up devices, including CCD's (Dalglish, James & Tubbenhauer, 1984), instead of the low-light-level camera tubes necessary with a lower pre-amplification.

An intensifier can, in principle, employ a variety of read-out methods, *e.g.* by substituting a resistive disc anode, a coded anode or a CCD for the output phosphor. However, the only way of employing standard modules is to couple them to a TV pick-up device.

7.1.6.5.4. *TV camera tubes*

Vacuum-tube television cameras have been largely replaced by semiconductor devices but of the former the preferred tube for use in an X-ray detector is still the silicon-intensifier-target (SIT) tube (Santilli & Conger, 1972). It has an adequate resolution for images up to 512×512 pixels and a linear transfer function (unity gamma) and its sensitivity is well matched for use with a single-stage image intensifier with a gain of 100. When cooled, this tube can be used for long exposures in an integrated slow read-out mode (Milch, Gruner & Reynolds, 1982).

When better high-gain image intensifiers become available, the preferred choice may be tubes like the Saticon (Goto, Isozaki, Shidara, Maruyama, Hirai & Fujita, 1974) whose diode gun gives them a superior resolution (Isozaki, Kumada, Okude, Oguso & Goto, 1981) and which have superior 'lag' or 'sticking' performance, that is a short 'memory' for previous high-intensity patterns to which they have been exposed (Shidara, Tanioka, Hirai & Nonaka, 1985).

7.1.6.6. *Some applications*

The use of linear and area detectors has increased markedly in recent years (Arndt, 1988). No new principles for the construction of linear devices have emerged, but more examples of each type have become commercially available.

Many more structures have been determined with area-detector diffractometers. The most commonly used gas-filled detectors at present are the delay-line read out MWPC first described by Xuong *et al.* (1978), as developed by Hamlin (1985), and a detector using a modification of the coded-anode read out due to Burns (Durbin, Burns, Moulai, Metcalf, Freymann, Blum, Anderson, Harrison & Wiley, 1986; Howard, Gilliland, Finzel, Poulos, Ohlendorf & Salemne, 1987; Derewenda & Helliwell, 1989). Corresponding instruments in the USSR and their use have been described by Anisimov, Zanevskii, Ivanov, Morchan, Peshekhonov, Chan Dyk Tkhan, Chan Khyo Dao, Cheremukhina & Chernenko (1986) and by Andrianova, Popov, Kheiker, Zanevskii, Ivanov, Peshekhonov & Chernenko (1986).

A two-dimensional photon-counting X-ray detector has been described by Collett & Podolsky (1988).

The widespread use of area-detector methods in single-crystal studies, especially for macromolecular material, has been greatly

aided by the development of complete software packages to deal with all aspects of data collection and handling. Earlier program packages (Howard, Nielson & Xuong, 1985; Pflugrath & Messerschmidt, 1987; Thomas, 1987) tended to be specific to one particular detector and its associated diffractometer. However, following the initiative of Bricogne (1987) and with financial assistance from EEC funds, a group of scientists, including most of the originators of the earlier packages, are now collaborating in writing, extending, and maintaining a comprehensive device-independent position-sensitive-detector software package.

Acknowledgements

Many helpful comments on this article by Drs A. R. Faruqi, H. E. Schwarz, and D. J. Thomas are gratefully acknowledged.

7.1.7. X-ray-sensitive TV cameras (By J. Chikawa)

High-resolution X-ray imaging systems are required for the topographic study of spatial change in crystal structures, such as that which takes place in phase transformations. From this point of view, high-resolution TV camera tubes will be described.

7.1.7.1. *Signal-to-noise ratio*

Video displays of X-ray and optical images have different features. Although X-ray photon energies are very large, the intensities available in X-ray diffraction are extremely low compared with optical images. Therefore, the photon noise resulting from the statistical fluctuation of the number of photons incident upon an image system gives a detection limit of the image.

Consider the case of defects in a crystal viewed by an imaging system: ν_p photons s^{-1} mm^{-2} are diffracted from the perfect region of a crystal, and $q\nu_p$ ($q < 1$) are absorbed by the X-ray-sensing layer of the system. An absorbed photon produces a mean number η_1 of electrons or visible photons, each of which may be rescattered to produce a mean number η_2 of electrons or photons. By repeating s such processes, the mean signal height

$$S_p = q\nu_p\eta_1\eta_2 \ldots \eta_s\delta^2 t \qquad (7.1.7.1)$$

is obtained from each square-shaped picture element $\delta \times \delta$ mm for t s. The value of δ may be taken as the limiting resolution of the system. Since $\eta_1 > 100$ owing to the large photon energy and the values of $\eta_2, \eta_3, \ldots, \eta_s$ are considered to be less than 100, the photon noise σ_p as a standard deviation of S_p is given by (Arcese, 1964)

$$\sigma_p = \eta_s\eta_{s-1} \ldots \eta_1(q\nu_p\delta^2 t)^{1/2}. \qquad (7.1.7.2)$$

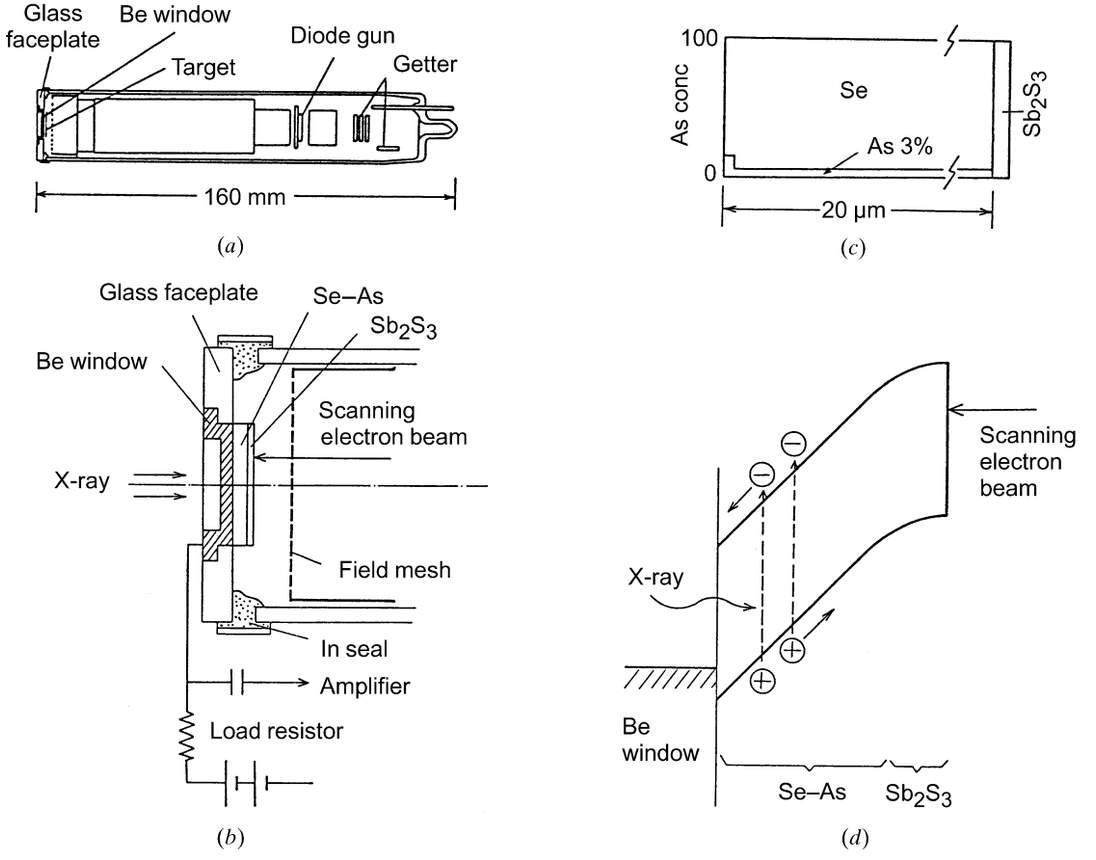

Fig. 7.1.7.1. Schematic illustration of an X-ray sensing Saticon camera tube. (*a*) Schematic representation of the tube. (*b*) Structure of the target. (*c*) Concentration (wt%) of As in the target (Se–As photoconductive layer). Since crystalline Se is metallic, As acts to stabilize the amorphous state. (*d*) Potential in the target. A blocking contact is formed between the X-ray window material and the Se–As alloy layer to prevent holes from flowing into the layer. Incident X-rays form electrons and holes in the layer, and the latter migrate toward the scanning-electron-beam side and contribute to the video signal. On the surface of the Se–As layer, Sb_2S_3 was evaporated to form another blocking contact that improves landing characteristics of the electron beam. By applying a high voltage on the layer, the holes are accelerated to produce multiplication (avalanche amplification), resulting in a great increase of the signal current.

In order to recognize the defect image in the perfect region, the signal-to-noise ratio (SNR) R_I of the image must be

$$R_I \equiv (S_d - S_p)/\sigma_p = \delta C(q\nu_p t)^{1/2} \geq \kappa, \qquad (7.1.7.3)$$

where S_d = signal height of the defect image, C = contrast of the defect image, $C = (S_d - S_p)/S_p$; and κ = threshold SNR of 1–5 (Rose, 1948).

Sensitivity is expressed by the intensity required for a certain signal height to the noise height of the imaging system and is proportional to the value of $q\eta_1 \ldots \eta_s$. As is seen from (7.1.7.3), however, the ratio of the signal to the photon noise depends only on the absorption efficiency q. For example, a 100 μm thick silicon-diode array (Rozgonyi, Haszlo & Statile, 1970) and 15 μm thick lead oxide camera tubes (Chikawa, 1974) have similar sensitivities for Mo $K\alpha$ radiation, but $q = 0.15$ and $q = 0.6$, respectively; the former obtains the sensitivity with a higher conversion efficiency ($\eta_1\eta_2 \ldots \eta_s$) of absorbed photon energy and gives a $(0.15/0.6)^{1/2} = 0.5$ times lower SNR.

It is clear from the foregoing discussion that imaging systems should be evaluated by three factors: resolution, integration time for observation, and SNR.

7.1.7.2. *Imaging system*

There are two kinds of imaging system (*e.g.* Green, 1977); one is a direct method in which X-ray input images are converted directly into video signals and the other is an indirect method in which X-ray images are first converted into visible-light images to be observed by the usual electro-optical system. In the latter, phosphor screens are widely used and the visible images can be magnified by a lens. However, the resolution is limited by the thickness of the phosphor screen that is required for a satisfactory absorption efficiency. In contrast, the direct method provides a high resolution.

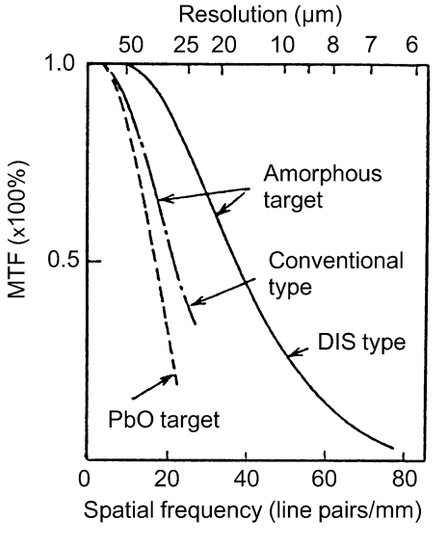

Fig. 7.1.7.2. Square-wave modulation transfer function (MTF) measured for the DIS-type, conventional-type Se–As and PbO camera tubes. This function shows the magnitude of brightness modulation in the output image obtained for an input image with a square-wave intensity distribution and is defined by

$$\mathrm{MTF} = \left(\frac{I_{o\max} - I_{o\min}}{I_{o\max} + I_{o\min}}\right)\left(\frac{I_{i\max} - I_{i\min}}{I_{i\max} + I_{i\min}}\right)^{-1},$$

where $I_{i\max}$ and $I_{i\min}$ are the maximum and minimum intensities of the input image, respectively, and $I_{o\max}$ and $I_{o\min}$ are those of the output. DIS stands for diode-operation impregnated-cathode Saticon.

Various types of indirect method are discussed in Subsections 2.7.5.2 and 7.1.6.5. Here only the direct method will be described in some detail.

A direct method using X-ray TV camera tubes has been used for real-time topography (Chikawa & Matsui, 1994). The construction and operation of an X-ray TV camera tube are similar to those of the conventional video pick-up tube, except for a beryllium window, as shown schematically in Fig. 7.1.7.1. The popular one is a vacuum glass tube which is 15 cm long and 25 mm in diameter. An X-ray sensing photoconductive layer such as Se (McMaster, Photen & Mitchell, 1967), or PbO (Chikawa, 1974) is placed on the inner surface of the window at one end of the tube and is scanned by a narrow electron beam from a cathode on the opposite end to convert image charges on the photoconductive layer into video signals. Therefore, the resolution depends upon the characteristics of the photoconductive layer and the electron-beam size on the layer.

The camera tube with a PbO photoconductive layer has absorption efficiencies of $q = 0.6$ for Mo $K\alpha$ and 0.8 for Cu $K\alpha$, using a PbO layer with a resolution-limited maximum thickness of 15 μm (Chikawa, 1974).

Dislocations in a silicon crystal were observed with the PbO camera tube and a high-power X-ray generator (tube voltage: 60 kV, current: 0.5 A) under the conditions $\nu_p =$

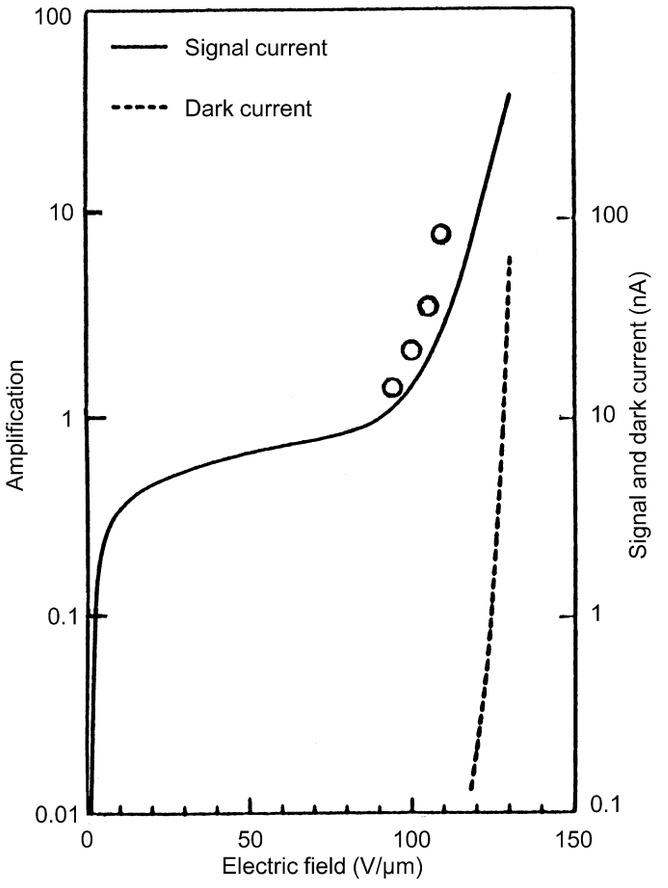

Fig. 7.1.7.3. Typical example showing dependence of the avalanche amplification on the electric field applied on the amorphous photoconductor (HARP). The solid and dashed lines show the amplification of signal current by visible light and dark current, respectively, for a 2 μm thick HARP layer. The right-hand scale shows the current (in nA). The open circles are the data for an 8 μm thick HARP layer by X-ray irradiation. Note that the thicker layer has higher amplifications owing to longer paths for running of holes.

4×10^{11} Mo $K\alpha_1$ photons s^{-1} m^{-2}, $C = 0.5$ and $\delta = 30$ μm (Chikawa, 1974) in (7.1.7.3). In order to improve the resolution further, q must be as high as possible even when ν_p is increased by 10–100 by use of synchrotron radiation, because R_I decreases with improving resolution (decreasing δ). (Note that C is not expected to increase much with improving resolution.) For example, to keep R_I at the same level as the previous case, q should be 0.7, say, for $\nu_p = 10^{13}$ photons s^{-1} m^{-2} and $\delta = 6$ μm. However, resolution and detection efficiency are, in general, mutually exclusive; the resolution of X-ray sensing photoconductive or phosphor materials is determined by the sizes of their grains and their sensitivities decrease with decreasing grain sizes. High resolution, without sacrificing detection efficiency, has been obtained with an amorphous Se–As alloy photoconductive layer, which has the advantage that no degradation of resolution occurs on increasing the layer thickness (Chikawa, Sato, Kawamura, Kuriyama, Yamashita & Goto, 1986). A layer with a thickness of 20 μm has an absorption efficiency of $q = 0.52$ for Mo $K\alpha$. The resolution of these tubes is shown with their modulation transfer functions in Fig. 7.1.7.2. The limiting resolution of 6 μm was obtained by making the scanning electron beam narrower with a diode-type electron gun have a barium-impregnated tungsten cathode (DIS type) (Chikawa, 1999). The Se–As layer shows very low lag characteristics (less than 1% after one frame).

This type of camera tube was developed primarily for TV broadcasting use and named 'Saticon' as the acronym for the components of the photoconductor, Se, As and Te. (Te enhances the sensitivity to red light.)

Such camera tubes have excellent linearity. The output signal current is proportional to the incident X-ray intensity up to 4 μA. The amplifier is always improving in signal-to-noise ratio, and, at present, the noise level of video amplifiers is ~0.2 nA; it is equivalent to an input intensity of $\sim 10^{11}$ Mo $K\alpha$ photons m^{-2} s^{-1} in the US/Japan standard scanning system (30 frames s^{-1}).

Therefore, it is important to increase conversion efficiency ($\eta_1, \eta_2, \ldots, \eta_s$). With increasing voltage applied on the photoconductive layer, the signal current is saturated (in Fig. 7.1.7.1, all the holes produced by an incident photon are collected), and then increases again further by avalanche amplification, as shown in Fig. 7.1.7.3; holes accelerated by a strong electric field cause their multiplication (Sato, Maruyama, Goto, Fujimoto, Shidara, Kawamura, Hirai, Sakai & Chikawa, 1993). It was referred to as 'HARP' (high-gain avalanche-rushing amorphous photoconductor). Together with the signal current, the dark current also increases as shown in Fig. 7.1.7.3. By allowing it to increase to the noise level of the video amplifier, an order of magnitude higher SNR can be achieved. Consequently, individual X-ray photons can be imaged as spots with a size resulting from the point-spread function, unless they are absorbed near the back surface of the photoconductive layer. For X-ray detection, a thick HARP layer should be employed with a very high applied voltage, and stable operation with avalanche amplification was confirmed for a 25 μm thick HARP layer. These pilot tubes were fabricated with a conventional electron gun and had a resolution of about 25 μm.

In general, avalanche amplification results in degradation of spatial resolution and has been used for zero-dimensional detection such as solid-state detectors. To make two-dimensional detection, isolation of each picture element is required. For the HARP, however, no appreciable degradation of resolution due to avalanche amplification was confirmed with a DIS-type tube having an 8 μm thick HARP layer by using visible light through a glass window. X-ray sensitive DIS-type tubes are now commercially available.

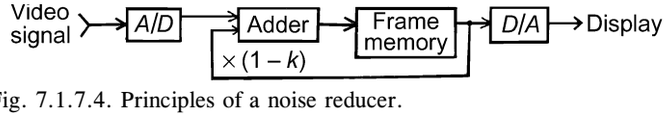

Fig. 7.1.7.4. Principles of a noise reducer.

7.1.7.3. *Image processing*

The resolution δ and integration time t should be selected appropriately according to experimental requirements (Chikawa, 1980). For example, when topographic images of a single dislocation in silicon were observed with $t = 1/30$ s by synchrotron radiation, their contrast and SNR were found to be $C = 0.5$ and $R_I = 20$ for $\delta = 30$ μm, and $C = 1$ and $R_I = 8$ for $\delta = 6$ μm. Since the SNR is desired to be 100, the integration time should be as large as possible unless images of moving objects are degraded. Digital image processing (Heynes, 1977) enables one to adjust the integration time easily. As an example, a noise reducer (McMann, Kreinik, Moore, Kaiser & Rossi, 1978; Rossi, 1978) is shown in Fig. 7.1.7.4. The video signal is sampled and digitized by the A/D converter and the digital video is sent to the adder and thence to the memory. Image information in the memory is continually sent both to the adder through the multiplier for combination with incoming data and to the display through the D/A converter. The weighting of new to old data is made by changing the factor k of the multiplier in the range $0 \le k \le 1$. For $k = 0$, the original input image is displayed. In the range $0 < k < 1$, a sliding summation of successive frames is displayed, and the SNR is improved by a factor of $[(1 + k)/(1 - k)]^{1/2}$. The factor k can be adjusted automatically by detecting the difference between successive frames.

Using a HARP tube, the SNR can be improved without integration of the amplifier noise by image processing, and topographs were displayed with an intensity of $\nu_p \simeq 10^9$ photons s^{-1} m^{-2} by a conventional X-ray generator.

Acquisition of extremely low intensity images, dramatic improvements in SNR *via* frame integration, and isolation and enhancement of selected-contrast ranges are possible by digital image processing (Chikawa & Kuriyama, 1991).

7.1.8. Storage phosphors (By Y. Amemiya and J. Chikawa)

A storage phosphor, called an 'imaging plate', is a two-dimensional detector having a high detective quantum efficiency (DQE) and a large dynamic range. It was developed in the early 1980's for diagnostic radiography (Sonoda, Takano, Miyahara & Kato, 1983; Kato, Miyahara & Takano, 1985). The performance characteristics of the imaging plate was quantitatively evaluated in the mid 1980's (Miyahara, Takahashi, Amemiya, Kamiya & Satow, 1986) and it was proved to be very useful also for X-ray diffraction experiments (Amemiya, Wakabayashi, Tanaka, Ueno & Miyahara, 1987; Amemiya & Miyahara, 1988). The imaging plate has replaced conventional X-ray film in many X-ray diffraction experiments.

The imaging plate (IP) is a flexible plastic plate that is coated with bunches of very small crystals (grain size about 5 μm) of photo-stimulable phosphor [previously BaFBr:Eu^{2+}, recently BaF(Br,I):Eu^{2+}] by using an organic binder. The photo-stimulable phosphor is capable of storing a fraction of the absorbed X-ray energy. When later stimulated by visible light, it emits photo-stimulated luminescence (PSL), the intensity of which is proportional to the absorbed X-ray intensity.

The mechanism of PSL is illustrated in Fig. 7.1.8.1. When the IP absorbs incoming X-rays, some of the electrons in the valence band are pumped up to the conduction band of the phosphor crystals. (This corresponds to ionization of Eu^{2+} to Eu^{3+}.) The electrons, in turn, are trapped in Br^- and F^- vacancies, which were intentionally introduced in the phosphor crystals during the manufacturing process, forming temporary colour centres, termed *F*-centres. Exposure to visible light again pumps up the trapped electrons so that they generate energy for luminescence, while returning to the valence band of the crystal. (This process corresponds to a recombination of electrons with Eu^{3+} ions, resulting in Eu^{2+} luminescence.) Because the response time of the PSL is as short as 0.8 μs, it is possible to read an X-ray image with a speed of 5–10 μs per pixel with high efficiency. The PSL is based on the allowable transition from $5d$ to $4f$ of Eu^{2+}. The wavelength of the PSL ($\lambda \simeq 390$ nm) is reasonably separated from that of the stimulating light ($\lambda = 632.8$ nm), allowing it to be collected by a conventional high-quantum-efficiency photomultiplier tube (PMT). The output of the PMT is amplified and converted to a digital image, which can be processed by a computer. The residual image on the IP can be completely erased by irradiation with visible light, to allow repeated use. The IP is easy to handle, because it is flexible, like a film, and can be kept in light before its exposure to X-rays.

The measured DQE of the IP is shown as a function of the X-ray exposure level together with that of a high-sensitivity X-ray film (Kodak DEF-5) in Fig. 7.1.8.2. The advantage of the IP over X-ray film in DQE is clearly enhanced at lower exposure levels. This arises from the fact that the background noise level of the IP is much smaller than that of X-ray film. The background noise level of the IP corresponds to the signal level of less than 3 X-ray photons/100 μm^2. This value compares favourably with the chemical 'fog' level of X-ray film, which amounts to 1000 X-ray photons per equivalent area. The background noise level of the IP depends largely on the performance of the IP read-out system, and it can be smaller than that of a single X-ray photon with a well designed IP read-out system (Amemiya, Matsushita, Nakagawa, Satow, Miyahara & Chikawa, 1988). The DQE of the IP decreases at higher exposure levels owing to 'system fluctuation noise'. Fig. 7.1.8.3 shows the fluctuation noise of the IP and X-ray film as a function of the X-ray exposure level. It is shown that the noise fluctuation at high exposure levels is governed by system fluctuation noise, which amounts to about 1%. Fig. 7.1.8.4 shows the propagation of signal and noise in the IP system. The origins of the system fluctuation noise are non-uniformity of absorption, non-uniformity of the colour-centre density, fluctuation of the laser intensity, non-uniformity of PSL collection, and fluctuation of the high-voltage supply to the PMT. Although it might be possible to reduce the total system fluctuation noise from ~1% to ~0.5%, it is very difficult to reduce it down to <0.1%. This means that the ultimate precision in intensity measurements with the IP is limited to the order of ~0.5%.

Compared to X-ray film, the dynamic range of the IP is much wider, of the order of 1:10^5 (Fig. 7.1.8.5). The response of the PSL is linear over the range from 8 to 40 000 photons/(100 μm^2), with an error rate of less than 5%. It is shown that the dynamic range of an IP is extended towards the lower exposure levels of X-ray film, but not to the higher exposure levels. The dynamic range of the IP is practically limited to four orders of magnitude by that of the PMT during the read-out. Two sets of PMT's are used in some read-out systems in order to cover the entire dynamic range of the IP.

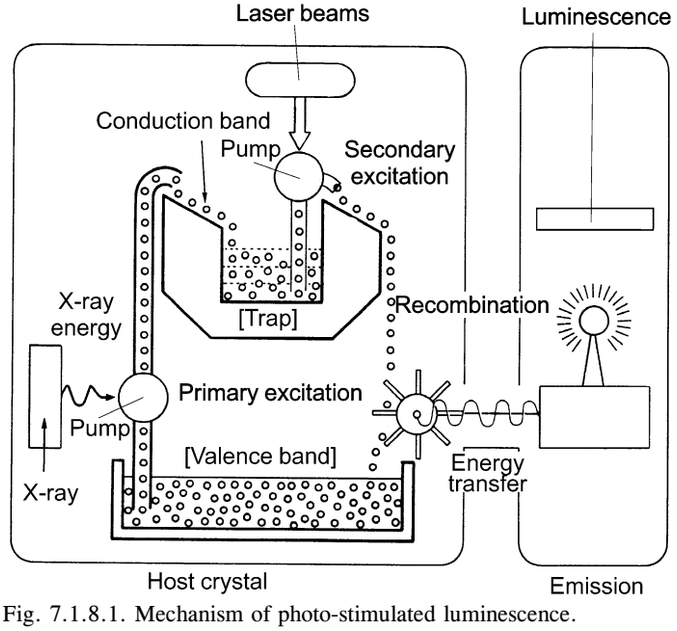

Fig. 7.1.8.1. Mechanism of photo-stimulated luminescence.

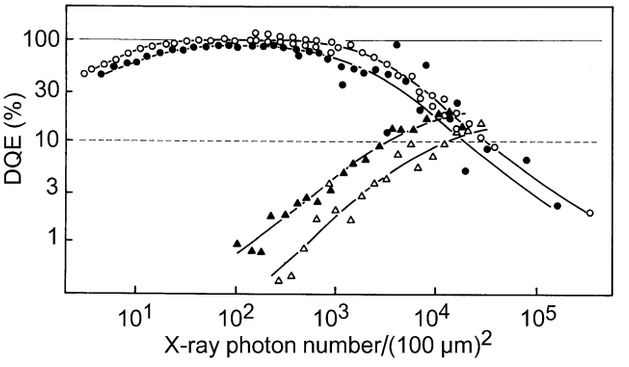

Fig. 7.1.8.2. Measured detective quantum efficiency (DQE) of the imaging plate and high-sensitivity X-ray film as a function of the exposure level. The circles correspond to the imaging plate (with the FCR 101 read-out system, Fuji Film Co. Ltd), triangles to the X-ray film (Kodak DEF-5). The filled symbols are for 8.9 keV and open symbols for 17.4 keV. The solid line indicates a noiseless counter of 100% absorption efficiency (ideal detector). The dashed line indicates a noiseless counter of 10% absorption efficiency (Amemiya & Miyahara, 1988).

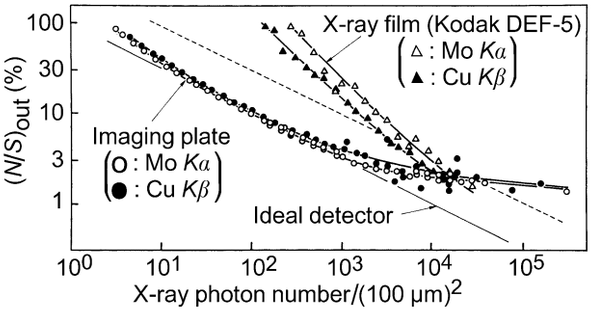

Fig. 7.1.8.3. Fluctuation noise in the signal as a function of the exposure level. The circles correspond to the imaging plate and the triangles to the X-ray film (Kodak DEF-5). The filled symbols are for 8.9 keV and the open symbols for 17.4 keV. The dashed line indicates a noiseless counter of 10% absorption efficiency (Miyahara, Takahashi, Amemiya, Kamiya & Satow, 1986).

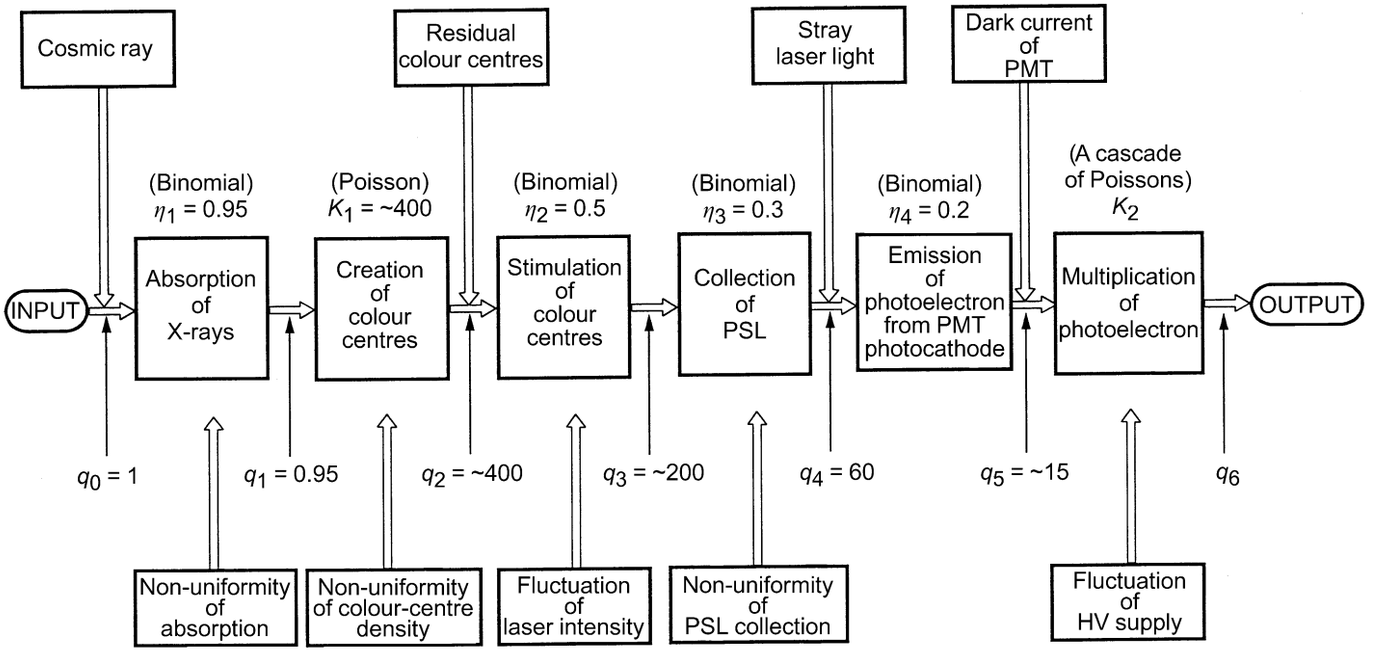

Fig. 7.1.8.4. Diagram showing a cascade of stochastic elementary processes during X-ray exposure and image read out of the imaging plate. The probability distribution of each stochastic process is described in parentheses together with the mean value. The numbers of the quanta, q_i ($i = 0, 5$), are also shown. The noise elements of the upper line contribute to the background noise, which reduces the DQE at lower exposure levels. The noise elements of the bottom line contribute to the system fluctuation noise, which reduces the DQE at higher exposure levels (Amemiya, 1995).

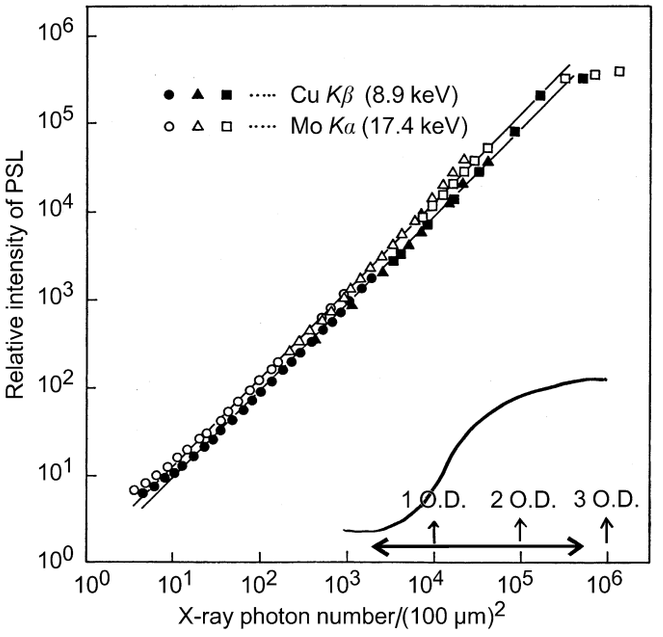

Fig. 7.1.8.5. Dynamic range of the photo-stimulated luminescence of the imaging plate. The dynamic range of typical high-sensitivity X-ray films is also shown. O.D. refers to optical density (Amemiya, 1995).

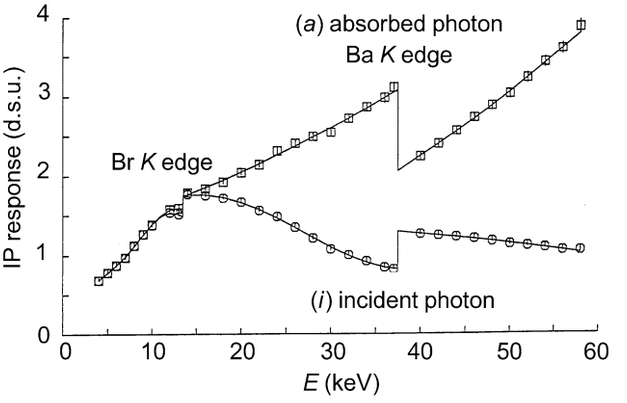

Fig. 7.1.8.6. Dependence of the IP response as a function of the energy of an X-ray photon. (*i*) is the IP response per an incident X-ray photon, and (*a*) the IP response per absorbed X-ray photon. The unit of the ordinate corresponds to the background noise level of the IP scanner (Ito & Amemiya, 1991).

The spatial resolution of the standard IP with a 100 μm laser scanning pitch is 170 μm at the full width at half-maximum (FWHM). The spatial resolution is limited by laser-light scattering in the phosphor during the read-out. A high-resolution IP that includes blue pigments in the phosphor to minimize the laser-light scattering has been developed. A spatial resolution of 43 μm is obtained at a 25 μm laser scanning pitch with the high-resolution IP with the sacrifice of 30% of the amount of PSL. The active area sizes of the available IP range from 127 × 127, 201 × 252, 201 × 400 to 800 × 400 mm.

The IP response per incident X-ray photon is shown as a function of the X-ray energy in Fig. 7.1.8.6, together with the deposited energy per absorbed X-ray photon. The abrupt decrease in the energy deposition above the barium *K*-absorption edge is due to the energy escape in the form of X-ray fluorescence. This effect is preferable because it makes the IP response curve smoother by compensating for the abrupt increase of the absorption efficiency at the absorption edge.

The image stored in the IP fades with the passage of time after exposure to X-rays. The fading rate depends on the type of IP and the temperature; it increases at higher temperature. But it does not depend on the exposure level or on the X-ray photon energy of the image. Fig. 7.1.8.7 shows the fading of an IP (type BAS III) as a function of time for two different X-ray energies at 293 K. The fading curve can be fitted well with three exponentials:

$$I(t) = A_1 \exp(-k_1 t) + A_2 \exp(-k_2 t) + A_3 \exp(-k_3 t).$$

$1/k_1$, $1/k_2$, and $1/k_3$ are 0.7, 18, and 520 h, respectively.

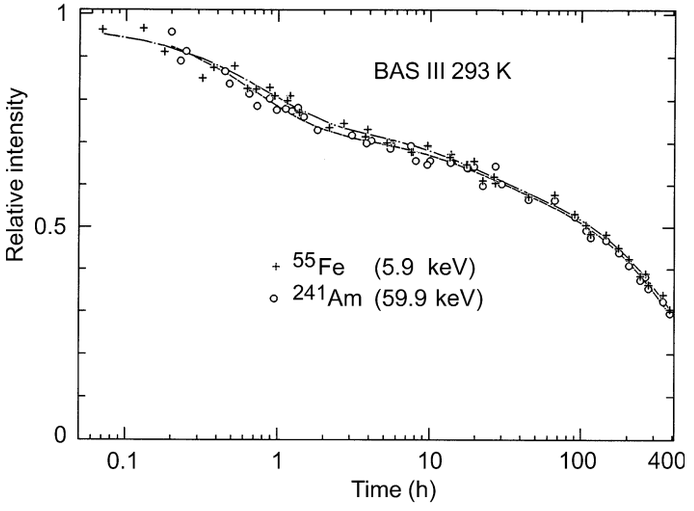

Fig. 7.1.8.7. Fading of the IP signals as a function of time with two different X-ray energies (5.9 and 59.5 keV). Temperature 293 K, type of IP: BAS III (Amemiya, 1995).

The non-uniformity of the response of the IP is about 1–2% over an active area of 250 × 200 mm. The distortion of the image is usually of the order 1%. It depends mainly on the type of IP read-out system.

Since the IP is an integrating-type detector, it is free from instantaneous count-rate limitations, which are accompanied by detectors operating in a pulse-counting mode. Therefore, the IP can make full use of a high flux of synchrotron X-radiation. Using synchrotron X-radiation, time-resolved measurements are possible by mechanically moving the IP (Amemiya, Kishimoto, Matsushita, Satow & Ando, 1989). Caution has been paid not to irradiate extremely intense X-rays (more than 10^6 photons μm^{-2}) on the IP; too intense X-rays create either non-erasable colour centres, or colour centres that are seemingly erasable but later reappear.

With minimum precautions, the IP yields reproducible results over a long period of repeated use, unlike X-ray film, whose performance is affected by slight changes in the development conditions. Various kinds of automated IP read-out systems are available, which permit on-site read-out in combination with an X-ray camera. The mechanical flexibility of the IP is also very important when it is used with a Weissenberg camera (Sakabe, 1991).

function of the measured intensities, say $F(I_1, I_2, \ldots, I_j, \ldots)$. General statistical theory gives the usual approximation

$$\sigma^2(F) = \sum_{i,j} \frac{\partial F}{\partial I_i}\frac{\partial F}{\partial I_j}\mathrm{cov}(I_i, I_j), \qquad (7.5.7.1)$$

where $\mathrm{cov}(I_i, I_j)$ is the covariance of I_i and I_j if $i \neq j$, and is the variance of I_j, $\sigma^2(I_j)$, if $i = j$. There is very little correlation* between successive intensity measurements in diffractometry, so that $\mathrm{cov}(I_i, I_j)$ is negligible for $i \neq j$. Equation (7.5.7.1) becomes

$$\sigma^2(F) = \sum_j \left(\frac{\partial F}{\partial I_j}\right)^2 \sigma^2(I_j). \qquad (7.5.7.2)$$

These equations are strictly accurate only if F is a linear function of the I's, a condition satisfied for the integrated intensity, but for few other quantities of interest. In most applications in diffractometry, however, the contribution of each I_j is sufficiently small in comparison with the total to make the application of equations (7.5.7.1) and (7.5.7.2) plausible. Any proportionality factors c_j (Section 7.5.1) can be absorbed into the functional relationship between F and the I_j's.

The object is to minimize $\sigma^2(F)$ by varying the time spent on each observation, subject to a fixed total time

$$T = \sum_j t_j. \qquad (7.5.7.3)$$

It is simplest to regard the total intensity and the background intensity as separate observations, so that in (7.5.7.2) the sum is over n 'background' and n 'total' observations. With I_j expressed as a counting rate, its variance is I_j/t_j [equation (7.5.3.8)], so that (7.5.7.2) becomes

$$\sigma^2(F) = \sum_j G_j^2 I_j/t_j, \qquad (7.5.7.4)$$

where for brevity G has been written for $|\partial F/\partial I|$. The variance of F will be a minimum if, for any small variations $\mathrm{d}t_j$ of the counting times t_j,

$$0 = -\sum_j G_j^2 I_j t_j^{-2}\,\mathrm{d}t_j, \qquad (7.5.7.5)$$

subject to the constancy of the total time T. There is thus the constraint

$$0 = \sum_j \mathrm{d}t_j. \qquad (7.5.7.6)$$

These equations are consistent if for all j

$$G_j^2 I_j t_j^{-2} = k^{-2}, \qquad (7.5.7.7)$$

$$t_j = k G_j I_j^{1/2}, \qquad (7.5.7.8)$$

where k is a constant determined by the total time T:

$$T = k\sum_j G_j I_j^{1/2}. \qquad (7.5.7.9)$$

The minimum variance is thus achieved if each observation is given a time proportional to the square root of its intensity. A little manipulation now gives for the desired minimum variance

$$\sigma^2_{\min}(F) = \frac{1}{T}\left[\sum_j \left(\partial F/\partial I_j\right) I_j^{1/2}\right]^2. \qquad (7.5.7.10)$$

The minimum variance is found to be a perfect square, and the standard uncertainty takes a simple form.

Here, the optimization has been treated as a modification of fixed-time counting. However, the same final expression is obtained if the optimization is treated as a modification of fixed-count timing (Wilson, Thomsen & Yap, 1965).

Space does not permit detailed discussion of the numerous papers on various aspects of optimization. If the time required to move the diffractometer from one observation position to another is appreciable, the optimization problem is affected (Shoemaker & Hamilton, 1972, and references cited therein). There is some dependence on the radiation (X-ray *versus* neutron) (Shoemaker, 1968; Werner 1972*a*,*b*). A few other papers of historical or other interest are included in the list of references, without detailed mention in the text: Grant (1973); Killean (1972, 1973); Mack & Spielberg (1958); Mackenzie & Williams (1973); Szabó (1978); Thomsen & Yap (1968); Zevin, Umanskii, Kheiker & Panchenko (1961).

* Exceptions to this statement may be important for line and area detectors, or if an interpolation function is used to estimate background. Wilson (1967) has discussed some features of the powder diffractometry case.

References

7.1.1

Hellner, E. (1954). *Intensitätsmessungen aus Aufnahmen in der Guinier-Kamera. Z. Kristallogr.* **106**, 122–145.

International Tables for X-ray Crystallography (1962). Vol. III. Birmingham: Kynoch Press.

Mees, C. E. K. (1954). *The theory of the photographic process*. New York: Macmillan.

Whittaker, E. J. W. (1953). *The Cox & Shaw factor. Acta Cryst.* **6**, 218.

7.1.2–7.1.4

Ames, L., Drummond, W., Iwanczyk, J. & Dabrowski, A. (1983). *Energy resolution measurements of mercuric iodide detectors using a cooled FET preamplifier. Adv. X-ray Anal.* **26**, 325–330.

Ballon, J., Comparat, V. & Pouxe, J. (1983). *The blade chamber: a solution for curved gaseous detectors. Nucl. Instrum. Methods*, **217**, 213–216.

Bish, D. L. & Chipera, S. J. (1989). *Comparison of a solid-state Si detector to a conventional scintillation detector–monochromator system in X-ray powder diffraction. Powder Diffr.* **4**, 137–143.

Eastabrook, J. N. & Hughes, J. W. (1953). *Elimination of dead-time corrections in monitored Geiger-counter X-ray measurements. J. Sci. Instrum.* **30**, 317–320.

Foster, B. A. & Wölfel, E. R. (1988). *Automated quantitative multiphase analysis using a focusing transmission diffractometer in conjunction with a curved position sensitive detector. Adv. X-ray Anal.* **31**, 325–330.

Geiger, H. & Müller, W. (1928). *Das Elektronenzählrohr. Z. Phys.* **29**, 839–841.

7.1.2–7.1.4 (*cont.*)

Göbel, H. E. (1982). *A Guinier diffractometer with a scanning position sensitive detector*. *Adv. X-ray Anal.* **25**, 315–324.

Heinrich, K. F. J., Newbury, D. E., Myklebust, R. L. & Fiori, C. E. (1981). Editors. *Energy dispersive X-ray spectrometry*. *US Natl Bur. Stand. Spec. Publ.* No. 604.

Kevex Corporation (1990). Brochure on equipment.

Kohler, T. R. & Parrish, W. (1955). *X-ray diffractometry of radioactive samples*. *Rev. Sci. Instrum.* **26**, 374–379.

Lehmann, M. S., Christensen, A. N., Fjellvåg, H., Feidenhans'l, R. & Nielsen, M. (1987). *Structure determination by use of pattern decomposition and the Rietveld method on synchrotron X-ray and neutron powder data; the structures of* $Al_2Y_4O_9$ *and* I_2O_4. *J. Appl. Cryst.* **20**, 123–129.

Nissenbaum, J., Levi, A., Burger, A., Schieber, M. & Burshtein, Z. (1984). *Supression of X-ray fluorescence background in X-ray powder diffraction by a mercuric iodide spectrometer*. *Adv. X-ray Anal.* **27**, 307–316.

Parrish, W. (1962). *Advances in X-ray diffractometry and X-ray spectrography*. Eindhoven: Centrex.

Parrish, W. (1966). *Escape peak interferences in X-ray powder diffractometry*. *Adv. X-ray Anal.* **8**, 118–133.

Parrish, W. & Kohler, T. R. (1956). *The use of counter tubes in X-ray analysis*. *Rev. Sci. Instrum.* **27**, 795–808.

Rigaku Corporation (1990). Brochure on equipment.

Russ, J. C. (1984). *Fundamentals of energy dispersive X-ray analysis*. London: Butterworth.

Shishiguchi, S., Minato, I. & Hashizume, H. (1986). *Rapid collection of X-ray powder data for pattern analysis by a cylindrical position-sensitive detector*. *J. Appl. Cryst.* **19**, 420–426.

Wölfel, E. R. (1983). *A novel curved position-sensitive proportional counter for X-ray diffractometry*. *J. Appl. Cryst.* **16**, 341–348.

7.1.5

Warburton, W. K., Iwanczyk, J. S., Dabrowski, A. J., Hedman, B., Penner-Hahn, J. E., Roe, A. L. & Hodgson, K. O. (1986). *Development of mercuric iodide detectors for XAS and XRD measurements*. *Nucl. Instrum. Methods*, A**246**, 558–560.

Worgan, J. S. (1982). *Energy-dispersive detectors for synchrotron radiation*. *Nucl. Instrum. Methods*, **201**, 85–91.

7.1.6

Airey, R. W. & Morgan, B. L. (1985). *A microchannel plate image intensifier for detection of photon-noise-limited images*. *IEE Conf. Publ. (London)*, **253**, 5–7.

Allemand, R. & Thomas, G. (1976). *New position-sensitive detectors: the 'backgammon' method*. *Nucl. Instrum. Methods*, **137**, 141–149.

Allington-Smith, J. R. & Schwarz, H. E. (1984). *Imaging photon detectors for optical astronomy, Q. J. R. Astron. Soc.* **25**, 267–289.

Allinson, N. M. (1982). *Solid-state imaging arrays for X-ray detection*. *Nucl. Instrum. Methods*, **201**, 53–64.

Allinson, N. M. (1994). *Development of non-intensified charge-coupled device area X-ray detectors*. *J. Synchrotron Rad.* **1**, 54–62.

Andrianova, M. E., Popov, A. N., Kheiker, D. M., Zanevskii, Yu. V., Ivanov, A. B., Peshekhonov, V. D. & Chernenko, S. P. (1986). *Use of coordinate X-ray diffractometer with a high-resolution chamber to obtain diffraction data for single crystals of proteins*. *Dokl. Akad. Nauk SSR,* **28**, 122–125. Translated in *Sov. Phys. Dokl. (USA)*, **31**, 358–361.

Anger, H. O. (1966). *Beam-position indentification means*. *Instrum. Soc. Am. Trans.* **5**, 311–334; US Patent 3 209 201.

Anisimov, Yu. S., Zanevskii, Yu. V., Ivanov, A. B., Morchan, V. D., Peshekhonov, V. D., Chan Dyk Tkhan, Chan Khyo Dao, Cheremukhina, G. A. & Chernenko, S. P. (1986). *Two-dimensional automated X-ray detector for diffraction experiments*. *Pribory i Tekhnika Eksperimenta*, No. 4, pp. 60–62. Translated in *Instrum. Exp. Tech.* **29**, 821–823.

Arndt, U. W. (1978). *Counting losses of detectors for X-rays from storage rings*. *J. Phys. E*, **11**, 671–673.

Arndt, U. W. (1982). *X-ray television area detectors*. *Nucl. Instrum. Methods*, **201**, 13–20.

Arndt, U. W. (1984). *Area detectors for protein crystallography at storage rings*. *Nucl. Instrum. Methods*, **222**, 252–255.

Arndt, U. W. (1985). *Television area detector diffractometers*. *Prog. Enzymol.* **114**, 472–485.

Arndt, U. W. (1986). *X-ray position-sensitive detectors*. *J. Appl. Cryst.* **19**, 145–163.

Arndt, U. W. (1988). *Position-sensitive detectors in condensed matter studies*. *Nucl. Instrum. Methods*, A**273**, 459–462.

Arndt, U. W. & Gilmore, D. J. (1979). *X-ray television area detectors for macromolecular structural studes with synchrotron radiation sources*. *J. Appl. Cryst.* **12**, 1–9.

Arndt, U. W., Gilmore, D. J. & Wonacott, A. J. (1977). *X-ray film. The rotation method in crystallography*, Chap. 14. Amsterdam: North Holland.

Arndt, U. W. & In't Veld, G. A. (1988). *Further developments of an X-ray television detector*. *Adv. Electron. Electron Phys.* **74**, 285–296.

Ballon, J., Comparat, V. & Pouxe, J. (1983). *The blade chamber: a solution for curved gaseous detectors*. *Nucl. Instrum. Methods*, **217**, 213–216.

Baru, S. E., Proviz, G. I., Savinov, G. A., Sidorov, V. A., Khabakhshev, A. G., Shuvalov, B. N. & Yakovlev, V. A. (1978). *Two-coordinate X-ray detector*. *Nucl. Instrum. Methods*, **152**, 209–212.

Bateman, J. E. & Apsimon, R. J. (1979). *A new photocathode for X-ray image intensifiers operating in the 1–50 keV region*. *Adv. Electron. Electron Phys.* **52**, 189–200.

Bigler, E., Polack, F. & Lowenthal, S. (1986). *Scintillating fibre array as an X-ray image detector*. *Proc. SPIE*, **733**, 133–137.

Bordas, J., Koch, M. J. H., Clout, P. N., Dorrington, E., Boulin, C. & Gabriel, A. (1980). *A synchrotron radiation camera and data acquisition system for time-resolved X-ray scattering studies*. *J. Phys. E*, **13**, 938–944.

Borkowski, C. J. & Kopp, M. K. (1968). *New type of position-sensitive detectors of ionizing radiation using rise-time measurement*. *Rev. Sci. Instrum.* **39**, 1515–1522.

Borso, C. S. (1982). *Optimisation of monolithic solid-state array detector for the position encoding of small-angle X-ray scattering from synchrotron sources*. *Nucl. Instrum. Methods*, **201**, 65–71.

Boulin, C., Dainton, D., Dorrington, E., Elsner, G., Gabriel, A., Bordas, J. & Koch, M. J. H. (1982). *Systems for time-resolved X-ray measurements using one-dimensional and two-dimensional detectors: requirements and practical experience*. *Nucl. Instrum. Methods*, **201**, 209–220.

Bricogne, G. (1987). *The EEC cooperative programming workshop on position-sensitive detector software. Computational aspects of protein crystal data analysis*, edited by J. R. Helliwell, P. A. Machin & M. Z. Papiz. SERC Daresbury Laboratory Report DL/SC1/R25, pp. 120–145.

7.1.6 (*cont.*)

Burke, B. E., Mountain, R. W., Harrison, D. C., Bautz, M. W., Doty, J. P., Ricker, G. R. & Daniels, P. J. (1991). *An abuttable CCD imager for visible and X-ray focal plane arrays. IEEE Trans. Electron Devices*, **38**, 1069–1076.

Charpak, G. (1982). *Parallax-free high-accuracy gaseous detectors for X-ray and VUV localization. Nucl. Instrum. Methods*, **201**, 181–192.

Chikawa, J., Sato, F. & Fujimoto, I. (1984). *High-resolution topography detector. Acta Cryst.* A**40**, C403.

Collett, B. & Podolsky, R. J. (1988). *2-D photon counter for X-ray imaging. Rev. Sci. Instrum.* **59**, 1122–1126.

Dalglish, R. L., James, V. J. & Tubbenhauer, G. A. (1984). *A 2-D X-ray diffraction pattern sensor using a solid-state area-sensitive detector. Nucl. Instrum. Methods*, **227**, 521–525.

Deckman, H. W. & Gruner, S. M. (1986). *Formal alterations in CCD-based electro-optic X-ray detectors. Nucl. Instrum. Methods*, A**246**, 527–533.

Dereniak, E. L., Roehrig, H., Salcido, M. M., Pommerrenig, D. H., Simms, R. A. & Abrahams, J. M. (1985). *Image intensifiers with electrical readout. IEE Conf. Publ. (London)*, **253**, 71–73.

Derewenda, Z. & Helliwell, J. R. (1989). *Calibration tests and use of Nicolet–Xentronics imaging proportional chamber mounted on a conventional source for protein crystallography. J. Appl. Cryst.* **22**, 123–137.

Durbin, R. M., Burns, R., Moulai, J., Metcalf, P., Freymann, D., Blum, M., Anderson, J. E., Harrison, S. C. & Wiley, D. C. (1986). *Protein, DNA and virus crystallography with a focused imaging proportional counter. Science*, **232**, 1127–1132.

Dyson, N. A. (1973). *X-rays in atomic & nuclear physics*. London: Longmans.

Eikenberry, E. F., Gruner, S. M. & Lowrance, J. L. (1986). *A two-dimensional X-ray detector with a slow-scan charge-coupled device readout. IEEE Trans. Nucl. Sci.* **33**, 542–545.

Emberson, D. L. & Holmshaw, R. T. (1972). *Some aspects of the design and performance of a small high-contrast channel image intensifier. Adv. Electron. Electron Phys.* **33**A, 133–144.

Fano, U. (1946). *On the theory of ionization yield of radiation in different substances. Phys Rev.* **70**, 44–52.

Fano, U. (1947). *Ionization yield of radiations: II. The fluctuations of the number of ions. Phys. Rev.* **72**, 26–29.

Faruqi, A. R. & Bond, C. C. (1982). *Multi-wire linear detector for X-ray time-resolved measurements at high counting rates. Nucl. Instrum. Methods*, **201**, 125–134.

Fordham, J. L. A., Bellis, J. G., Bone, D. A. & Norton, T. J. (1991). *The MIC photon-counting detector. Proc. SPIE*, **1449**, 87–98.

Fouassier, M., Duchenois, V., Dietz, J., Guillemet, E. & Lemonnier, M. (1988). *Image intensifier tubes with intagliated screens. Adv. Electron. Electron Phys.* **74**, 315–322.

Fraser, G. W. (1989). *X-ray detectors: a review. Proc. SPIE*, **1140**, 50–57.

Fuchs, H. F., Wu, D. Q. & Chu, B. (1990). *An area X-ray detector system based on a commercially available CCD unit. Rev. Sci. Instrum.* **61**, 712–716.

Gabriel, A. & Dupont, Y. (1972). *A position-sensitive proportional detector for X-ray crystallography. Rev. Sci. Instrum.* **43**, 1600–1602.

Garfield, B. R. C., Wilson, R. J. F., Goodson, J. H. & Butler, D. J. (1976). *Developments in proximity-focused diode image intensifiers. Adv. Electron. Electron Phys.* **40**A, 11–20.

Goto, N., Isozaki, Y., Shidara, K., Maruyama, E., Hirai, T. & Fujita, T. (1974). *Saticon: a new photoconductive camera tube with Se–As–Te target. IEEE Trans. Electron Devices*, ED-**21**, 662–666.

Gruner, S. M. & Milch, J. R. (1982). *Criteria for the evaluation of 2-dimensional X-ray detectors. Trans. Am. Crystallogr. Assoc.* **18**, 149–167.

Gruner, S. M., Milch, J. R. & Reynolds, G. T. (1982). *Survey of two-dimensional electro-optical X-ray detectors. Nucl. Instrum. Methods*, **195**, 287–297.

Hamlin, R. (1985). *Multiwire area X-ray diffractometers. Methods Enzymol.* **114**, 416–452.

Hasegawa, K., Mochiki, K. & Sekiguchi, A. (1981). *Integral type position-sensitive X-ray detector for high-flux diffuse scattering applications. IEEE Trans. Nucl. Sci. NS-***28**, 3660–3664.

Haubold, H. G. (1984). *An integrating 2-D position-sensitive X-ray detector for high-flux diffuse scattering applications*. Communication to ESRP Working Party on Detectors.

Hendricks, R. W. (1976). *One- and two-dimensional position-sensitive X-ray and neutron detectors. Trans. Am. Crystallogr. Assoc.* **12**, 103–146.

Hendricks, R. W., Seeger, P. A., Scheer, J. W. & Suehiro, S. (1982). *A large-capacity high-speed multiparameter multi-channel analysis system. Nucl. Instrum. Methods*, **201**, 261–279.

Hendrix, J. (1982). *Position-sensitive X-ray detectors. Uses of synchrotron radiation in biology*, edited by H. B. Stuhrmann, Chap. 11. New York: Academic Press.

Hendrix, J. (1984). *The fine-grid detector: a parallel-electrode position-sensitive detector. IEEE Trans. Nucl. Sci.* NS-**31**, 281–284.

Hopf, R. & Rodricks, B. (1994). *A VXI-based high-speed X-ray CCD detector. Nucl. Instrum. Methods*, A**348**, 645–648.

Howard, A. J., Gilliland, G. L., Finzel, B. C., Poulos, T. L., Ohlendorf, D. H. & Salemne, F. R. (1987). *The use of an imaging proportional counter in macromolecular crystallography. J. Appl. Cryst.* **20**, 383–387.

Howard, A. J., Nielson, C. & Xuong, Ng. H. (1985). *Software for a diffractometer with multiwire area detector. Methods Enzymol.* **114**, 452–472.

Howes, M. J. & Morgan, D. V. (1979). Editors. *Charge-coupled devices and systems*. New York: John Wiley.

Hughes, G. & Sumner, I. (1981). *DL100 memory system*. Daresbury Laboratory Report DL/CSE/TM2.

Huxley, H. E. & Faruqi, A. R. (1983). *Time-resolved X-ray diffraction studies on vertebrate striated muscle. Annu. Rev. Biophys. Bioeng.* **12**, 381–417.

Ikhlef, A. & Skowronek, M. (1993). *Radiation position-sensitive detector based on plastic scintillating fibres. Rev. Sci. Instrum.* **61**, 2566–2569.

Ikhlef, A. & Skowronek, M. (1994). *Some emission characteristics of scintillating fibres for low-energy X- and Y-rays. IEEE Trans. Nucl. Sci.* NS-**41**, 408–414.

Isozaki, Y., Kumada, J., Okude, S., Oguso, C. & Goto, N. (1981). *One-inch saticon for high-definition color television cameras. IEEE Trans. Electron Devices*, ED-**28**, 1500–1507.

Jones, R. C. (1958). *On the quantum efficiency of photographic negatives. Photogr. Sci. Eng.* **2**, 57–65.

Jucha, A., Bonin, D., Dartyge, E., Flank, A. M., Fontaine, A. & Raoux, D. (1984). *Photodiode array for position-sensitive detection using high X-ray flux provided by synchrotron radiation. Nucl. Instrum. Methods*, **226**, 40–45.

7.1.6 (*cont.*)

Kahn, R., Fourme, R., Bosshard, R., Caudron, B., Santiard, J. C. & Charpak, G. (1982). *An X-ray diffractometer for macromolecular crystallography based on a spherical drift chamber: hardware, software and multi-wavelength data acquisition with synchrotron radiation. Nucl. Instrum. Methods*, **201**, 203–208.

Kalata, K. (1982). *A versatile television X-ray detector and image processing system. Nucl. Instrum. Methods*, **201**, 35–41.

Kalata, K. (1985). *A general-purpose computer-configurable television area detector for X-ray diffraction applications. Prog. Enzymol.* **114**, 486–510.

Karellas, A., Liu, H., Harris, L. J. & D'Orsi, C. J. (1992). *Operational characteristics and potential of scientific-grade CCD in X-ray imaging applications. Proc. SPIE*, **1655**, 85–91.

Knibbeler, C. L. C. M., Hellings, G. J. A., Maaskamp, H. J., Ottewanger, H. & Brongersma, H. H. (1987). *Novel two-dimensional positional-sensitive detection system. Rev. Sci. Instrum.* **58**, 125–126.

Koch, A. (1994). *Lens-coupled scintillating screen CCD X-ray area detector with a high DQE. Nucl. Instrum. Methods*, A**348**, 654–658.

Lemonnier, M., Richard, J. C., Piaget, C., Petit, M. & Vittot, M. (1985). *Photon-in and electron-in CCD arrays for image read-out in tubes. IEE Conf. Publ. (London)*, **253**, 74–76.

Lewis, R. (1994). *Multiwire gas proportional counters: decrepit antiques or classic performers? J. Synchrotron Rad.* **1**, 43–53.

Lowrance, J. L. (1979). *A review of solid-state image sensors. Adv. Electron. Electron Phys.* **52**, 421–429.

Lowrance, J. L., Zucchino, P., Renda, G. & Long, D. C. (1979). *ICCD development at Princeton. Adv. Electron. Electron Phys.* **52**, 441–452.

Lumb, D. H., Chowanietz, E. G. & Wells, A. A. (1985). *X-ray imaging with GEC/EEV CCD's. IEE Conf. Publ. (London)*, **253**, Suppl.

Martin, C., Jelinsky, P., Lampton, M., Malina, R. F. & Anger, H. O. (1981). *Wedge-and-strip anodes for centroid-finding position-sensitive photon and particle detectors. Rev. Sci. Instrum.* **52**, 1067–1074.

Matsushima, I., Koyama, K., Tanimoto, M. & Yano, Y. (1987). *Soft X-ray imaging by a commercial solid state TV camera. Rev. Sci. Instrum.* **58**, 600–603.

Meyer-Ilse, W., Wilhelm, T. & Guttmann, P. (1993). *Thinned back-illuminated CCD for X-ray microscopy. Proc. SPIE*, **1900**, 241–245.

Milch, J. R., Gruner, S. M. & Reynolds, G. T. (1982). *Area detectors capable of recording X-ray diffraction patterns at high counting rates. Nucl. Instrum. Methods*, **201**, 43–52.

Miyahara, J., Takahashi, K., Amemiya, Y., Kamiya, N. & Satow, Y. (1986). *A new type of X-ray area detector utilizing laser-stimulated luminescence. Nucl. Instrum. Methods*, A**426**, 572–578.

Mochiki, K. (1984). *Integral type position-sensitive proportional chamber*. Dissertation, Faculty of Engineering, University of Tokyo, Japan.

Mochiki, K. & Hasegawa, K. (1985). *Charge-integrating type position-sensitive proportional chamber of time-resolved measurements using intense X-ray sources. Nucl. Instrum. Methods*, A**234**, 593–601.

Mochiki, K., Hasegawa, K., Sekiguchi, A. A. & Yoshioka, Y. (1981). *Integral type position-sensitive proportional chamber with multiplexer read-out system for X-ray diffraction experiments. Adv. X-ray Anal.* **24**, 155–159.

Moy, J.-P. (1994). *A 200 mm input field 5–80 keV detector based on an X-ray image intensifier and CCD camera. Nucl. Instrum. Methods*, A**348**, 641–644.

Naday, I., Westbrook, E. M., Westbrook, M. L., Travis, D. J., Stanton, M., Phillips, W. C., O'Mara, D. & Xie, J. (1994). *Nucl. Instrum. Methods*, A**348**, 635–640.

Oba, K., Ito, M., Yamaguchi, M. & Tanaka, M. (1988). *A CsI(Na) scintillation plate with high spatial resolution. Adv. Electron. Electron Phys.* **74**, 247–255.

Patt, B. E., Delduca, A., Dolin, R. & Ortale, C. (1986). *Mercuric iodide X-ray camera. IEEE Trans. Nucl. Sci.* NS-**33**, 523–526.

Peisert, A. (1982). *The parallel-plate avalanche chamber as an endcap detector for time-projection chambers. Nucl. Instrum. Methods*, **217**, 229–235.

Pernot, P., Kahn, R., Fourme, R., Leboucher, P., Million, G., Santiard, J. C. & Charpak, G. (1982). *A high count rate one-dimensional position-sensitive detector and a data acquisition system for time-resolved X-ray scattering studies. Nucl. Instrum. Methods*, **201**, 145–151.

Pflugrath, J. W. & Messerschmidt, A. (1987). *FAST system software. Computational aspects of protein crystal data analysis*, edited by J. R. Helliwell, P. A. Machin & M. Z. Papiz. SERC Daresbury Laboratory Report DL/SC1/R25, pp. 149–161.

Phizackerley, R. P., Cork, C. W. & Merritt, E. A. (1986). *An area detector data acquisition system for protein crystallography using multiple-energy anomalous dispersion techniques. Nucl. Instrum. Methods*, A**246**, 579–595.

Pollehn, H. K. (1985). *Performance and reliability of third-generation image intensifiers. Adv. Electron. Electron Phys.* **64**A, 61–69.

Price, W. J. (1964). *Nuclear radiation detectors*. New York: McGraw-Hill.

Rice-Evans, P. (1974). *Spark, streamer, proportional and drift chambers*. London: Richelieu Press.

Roehrig, H., Dallas, W. J., Ovitt, T. W., Lamoreaux, R. D., Vercillo, R. & McNeill, K. M. (1989). *A high-resolution X-ray imaging device. Proc SPIE*, **1072**, 88–99.

Rose, A. (1946). *A unified approach to the performance of photographic film, television pick-up tubes and the human eye. J. Soc. Motion Pict. Eng.* **47**, 273–294.

Sakabe, N. (1991). *X-ray diffraction data collection system for modern protein crystallography with a Weissenberg camera and an imaging plate using synchrotron radiation. Nucl. Instrum. Methods*, A**303**, 448–463.

Santilli, V. J. & Conger, G. B. (1972). *TV camera with large silicon diode array targets operating in the electron-bombarded mode. Adv. Electron. Electron. Phys.* **33**A, 219–228.

Sareen, R. A. (1994). *Developments in X-ray detectors and associated electronics: a review of the technology and possible future trends. J. X-ray Sci. Technol.* **4**, 151–165.

Sato, F., Maruyama, H., Goto, K., Fujimoto, I., Shidara, K., Kawamura, T. W., Hirai, T., Sakai, H. & Chikawa, J. (1993). *Characteristics of a new high-sensitivity X-ray imaging tube for video topography. Jpn. J. Appl. Phys.* **32**, 2142–2146.

Schwarz, H. E. & Lapington, J. S. (1985). *Optimisation of wedge-and-strip anodes. IEEE Trans. Nucl. Sci.* NS-**32**, 433–437.

7.1.6 (*cont.*)

Schwarz, H. E. & Mason, I. M. (1984). *A new imaging proportional counter using a Penning gas improves energy resolution. Nature (London)*, **309**, 532–534.

Schwarz, H. E. & Mason, I. M. (1985). *Development of the Penning-gas imager. IEEE Trans. Nucl. Sci.* NS-**32**, 516–520.

Shidara, K., Tanioka, K., Hirai, T. & Nonaka, Y. (1985). *Recent improvement of Saticon target. IEE Conf. Publ. (London),* **253**, 29–32.

Siegmund, O. H. W., Culhane, J. L., Mason, I. M. & Sanford, P. W. (1982). *Individual electrons detected after the interaction of ionizing radiation with gases. Nature (London)*, **295**, 678–679.

Smith, G. (1984). *High-accuracy gaseous X-ray detectors. Nucl. Instrum. Methods*, **222**, 230–237.

Sonada, M., Takano, M., Miyahara, J. & Kato, H. (1983). *Computed radiography utilizing scanning laser-stimulated luminescence. Radiology*, **148**, 833–838.

Stanton, M. (1993). *Area detector design I. Nucl. Instrum. Methods*, A**325**, 550–557.

Stanton, M., Phillips, W. C., Li, Y. & Kalata, K. (1992*a*). *DQE of CCD- and vidicon-based detectors for X-ray crystallographic applications. J. Appl. Cryst.* **25**, 638–645.

Stanton, M., Phillips, W. C., Li, Y. & Kalata, K. (1992*b*). *Correcting spatial distortion and non-uniform response in area detectors. J. Appl. Cryst.* **25**, 549–558.

Stanton, M., Phillips, W. C., O'Mara, D., Naday, I. & Westbrook, E. M. (1993). *Area detector design II. Nucl. Instrum. Methods*, A**325**, 558–567.

Strauss, M. G., Naday, I., Sherman, I. S., Kraimer, M. R. & Westbrook, E. M. (1987). *CCD-based synchrotron X-ray detector for protein crystallography. IEEE Trans. Nucl. Sci.* NS-**34**, 389–395.

Strauss, M. G., Westbrook, E. M., Naday, I., Coleman, T. A., Westbrook, M. L., Travis, D. J., Sweet, R. M., Pflugrath, J. W. & Stanton, M. (1990). *A CCD-based detector for protein crystallography. Nucl. Instrum. Methods*, A**297**, 275–295.

Stümpel, J. W., Sanford, P. W. & Goddard, H. F. (1973). *A position-sensitive proportional counter with high spatial resolution. J. Phys. E*, **6**, 397–400.

Suzuki, Y., Hayakawa, K., Usami, K., Hirano, T., Endoh, T. & Okamura, Y. (1989). *X-ray sensing pick-up tube. Rev. Sci. Instrum.* **60**, 2299–2302.

Suzuki, Y., Uchiyama, K. & Ito, M. (1976). *A large-diameter X-ray sensitive vidicon with beryllium window. Adv. Electron. Electron Phys.* **40**A, 209–222.

Symposia on Photoelectronic Imaging Devices (1960, 1962, 1966, 1969, 1972, 1976, 1979, 1985). Imperial College, London. *Adv. Electron. Electron Phys.* **12** (1st, 1960), **16** (2nd, 1962), **22** (3rd, 1966), **28** (4th, 1969), **33** (5th, 1972), **40** (6th, 1976), **52** (7th, 1979), **64** (8th, 1985).

Templer, R. H., Gruner, S. M. & Eikenberry, E. F. (1988). *An image-intensified CCD area X-ray detector for use with synchrotron radiation. Adv. Electron. Electron Phys.* **74**, 275–283.

Third European Symposium on Semiconductor Detectors (1984). *New developments in silicon detectors. Nucl. Instrum. Methods*, **226**.

Thomas, D. J. (1987). *The balance between the relative capabilities of X-ray area detectors, computer and interface hardware and software packages. Computation aspects of protein crystal data analysis*, edited by J. R. Helliwell, P. A. Machin & M. Z. Papiz. SERC Daresbury Laboratory Report DL/SC1/R25, pp. 162–166.

Thomas, D. J. (1989). *Calibrating an area-detector diffractometer: imaging geometry. Proc. R. Soc. London Ser. A*, **425**, 129–167.

Thomas, D. J. (1990). *Calibrating an area detector diffractometer: integral response. Proc. R. Soc. London Ser. A*, **428**, 181–214.

Walton, D., Stern, R. A., Catura, R. C. & Culhane, J. L. (1985). *Deep-depletion CCD's for X-ray astronomy. SPIE Proc.* **501**.

Widom, J. & Feng, H.-P. (1989). *High-performance X-ray area detector suitable for small-angle scattering, crystallographic and kinetic studies. Rev. Sci. Instrum.* **60**, 3231–3238.

Wilkinson, D. H. (1950). *Ionisation Chambers & Counters.* Cambridge University Press.

Wölfel, E. R. (1983). *A novel curved position-sensitive proportional counter for X-ray diffractometry. J. Appl. Cryst.* **16**, 341–348.

Xuong, Ng. H., Freer, S. T., Hamlin, R., Neilsen, C. & Vernon, W. (1978). *The electronic stationary-picture method for high-speed measurement of reflection intensities from crystals with large unit cells. Acta Cryst.* A**34**, 289–296.

7.1.7

Arcese, A. (1964). *A note on Poisson branching processes with reference to photon–electron converters. Appl. Opt.* **3**, 435.

Chikawa, J. (1974). *Technique for the video display of X-ray topographic images and its application to the study of crystal growth. J. Cryst. Growth*, **24/25**, 61–68.

Chikawa, J. (1980). *Laboratory techniques for transmission X-ray topography. Characterization of crystal growth defects by X-ray methods*, edited by B. K. Tanner & D. K. Bowen, Chap. 15, pp. 368–400. New York: Plenum.

Chikawa, J. (1999). *Live X-ray topography and crystal growth of silicon. Jpn. J. Appl. Phys.* **3**, 4619–4631.

Chikawa, J. & Kuriyama, M. (1991). *Topography. Handbook on synchrotron radiation*, Vol. 3, edited by G. Brown & D. E. Moncton, Chap. 10, pp. 337–378. Amsterdam: Elsevier.

Chikawa, J. & Matsui, J. (1994). *Growth and evaluation of bulk crystals. Handbook on semiconductors*, completely revised edition, Vol. 3, edited by S. Mahajan, Chap. 1, pp. 1–71. Amsterdam: Elsevier.

Chikawa, J., Sato, F., Kawamura, T., Kuriyama, T., Yamashita, T. & Goto, N. (1986). *A high-resolution video camera tube for live X-ray topography using synchrotron radiation. X-ray instrumentation for the Photon Factory: dynamic analyses of micro structures in matter*, edited by S. Hosoya, Y. Iitaka & H. Hashizume, pp. 145–157. Tokyo: KTK Scientific Publishers.

Green, R. E. Jr (1977). *Direct display of X-ray topographic images. Adv. X-ray Anal.* **20**, 221–235.

Heynes, G. D. (1977). *Digital television; a glossary and bibliography. SMPTE J.* **86**, 6–9.

McMann, R. H., Kreinik, S., Moore, J. K., Kaiser, A. & Rossi, J. (1978). *A digital noise reducer for encoded NTSC signals. SMPTE J.* **87**, 129–133.

McMaster, R. C., Photen, M. L. & Mitchell, J. P. (1967). *The X-ray vidicon television image system. Mater. Eval.* **25**, 46–52.

Rose, A. (1948). *The sensitivity performance of the human eye on an absolute scale. J. Opt. Soc. Am.* **38**, 196–208.

7.1.7 (*cont.*)

Rossi, J. P. (1978). *Digital technique for reducing television noise*. *SMPTE J.* **87**, 134–140.

Rozgonyi, G. A., Haszlo, S. E. & Statile, J. L. (1970). *Instantaneous video display of X-ray topographic images with resolving capabilities better than 15*. *Appl. Phys. Lett.* **16**, 443–446.

Sato, F., Maruyama, H., Goto, K., Fujimoto, I., Shidara, K., Kawamura, T., Hirai, T., Sakai, H. & Chikawa, J. (1993). *Characteristics of a new high-sensitivity X-ray imaging tube for video topography*. *Jpn. J. Appl. Phys.* **32**, 2142–2146.

7.1.8

Amemiya, Y. (1995). *Imaging plates for use with synchrotron radiation*. *J. Synchrotron Rad.* **2**, 13–21.

Amemiya, Y., Kishimoto, S., Matsushita, T., Satow, Y. & Ando, M. (1989). *Imaging plate for time-resolved X-ray measurements*. *Rev. Sci. Instrum.* **60**, 1552–1556.

Amemiya, Y., Matsushita, T., Nakagawa, A., Satow, Y., Miyahara, J. & Chikawa, J. (1988). *Design and performance of an imaging plate system for X-ray diffraction study*. *Nucl. Instrum. Methods*, A**266**, 645–653.

Amemiya, Y. & Miyahara, J. (1988). *Imaging plate illuminates many fields*. *Nature (London)*, **336**, 89–90.

Amemiya, Y., Wakabayashi, K., Tanaka, H., Ueno, Y. & Miyahara, J. (1987). *Laster-stimulated luminescence used to measure X-ray diffraction of a contracting striated muscle*. *Science*, **237**, 164–168.

Ito, M. & Amemiya, Y. (1991). *X-ray energy dependence and uniformity of an imaging plate detector*. *Nucl. Instrum. Methods*, A**310**, 369–372.

Kato, H., Miyahara, J. & Takano, M. (1985). *New computed radiography using scanning laser stimulated luminescence*. *Neurosurg. Rev.* **8**, 53–62.

Miyahara, J., Takahashi, K., Amemiya, Y., Kamiya, K. & Satow, Y. (1986). *A new type of X-ray area detector utilizing laser stimulated luminescence*. *Nucl. Instrum. Methods*, A**246**, 572–578.

Sakabe, N. (1991). *X-ray diffraction data collection system for modern protein crystallography with a Weissenberg camera and an imaging plate using synchrotron radiation*. *Nucl. Instrum. Methods*, A**303**, 448–463.

Sonoda, M., Takano, M., Miyahara, J. & Kato, H. (1983). *Computed radiography utilizing scanning laser stimulated luminescence*. *Radiology*, **148**, 833–838.

7.2

Burge, R. E. & van Toorn, P. (1980). *Multiple images and image processing in STEM*. *Scanning Electron Microscopy/* 1980, Vol. 1, pp. 81–91. AMF O'Hare/Chicago: SEM Inc.

Chapman, J. N., Craven, A. J. & Scott, C. P. (1989). *Electron detection in the analytical electron microscope*. *Ultramicroscopy,* **28**, 108–117.

Chapman, J. N. & Morrison, G. R. (1984). *Detector systems for transmission electron microscopy*. *J. Microsc. Spectrosc. Electron.* **9**, 329–340.

Craven, A. J. & Buggy, T. W. (1984). *Correcting electron energy loss spectra for artefacts introduced by a serial data collection system*. *J. Microsc.* **136**, 227–239.

Daberkow, L., Herrmann, K.-H., Liu, L. & Rau, W. D. (1991). *Performance of electron image convertors with YAG single-crystal screen and CCD sensor*. *Ultramicroscopy*, **38**, 215–223.

Fan, G. Y. & Ellisman, M. H. (1993). *High-sensitivity lens-coupled slow-scan CCD camera for transmission electron microscopy*. *Ultramicroscopy*, **52**, 21–29.

Farnell, G. C. & Flint, R. B. (1975). *Photographic aspects of electron microscopy*. *Principles and techniques of electron microscopy*, Vol. 5, edited by M. A. Hayat, pp. 19–61. New York: Van Nostrand Rheinhold.

Garlick, G. F. J. (1966). *Cathodo- and radioluminescence*. *Luminescence of inorganic solids*, edited by P. Goldberg, Chap. 12. London: Academic Press.

Guetter, E. & Menzel, M. (1978). *An external photographic system for electron microscopes*. *Electron microscopy 1978*, Vol. 1, edited by J. M. Sturgess, pp. 92–93. Toronto: Microscopical Society of Canada.

Hamilton, J. F. & Marchant, J. C. J. (1967). *Image recording in electron microscopy*. *J. Opt. Soc. Am.* **57**, 232–239.

Herrmann, K.-H. (1984). *Detection systems*. *Quantitative electron microscopy*, edited by J. N. Chapman & A. J. Craven, Chap. 4. Edinburgh University Press.

Herrmann, K.-H. & Krahl, D. (1984). *Electronic image recording in conventional electron microscopy*. *Advances in optical and electron microscopy*, edited by R. Barer & V. E. Cosslett, Chap. 1. London: Academic Press.

Ishizuka, K. (1993). *Analysis of electron image detection efficiency of slow-scan CCD cameras*. *Ultramicroscopy*, **52**, 7–20.

Isoda, S., Saitoh, K., Moriguchi, S. & Kobayashi, T. (1991). *Utility test of image plate as a high-resolution image-recording material for radiation-sensitive specimens*. *Ultramicroscopy*, **35**, 329–338.

Krivanek, O. L., Ahn, C. C. & Keeney, R. B. (1987). *Parallel detection electron spectrometer using quadrupole lenses*. *Ultramicroscopy*, **22**, 103–115.

Kujawa, S. & Krahl, D. (1992). *Performance of a low-noise CCD camera adapted to a transmission electron microscope*. *Ultramicroscopy*, **46**, 395–403.

Mori, N., Katoh, T., Oikawa, T., Miyahara, J. & Harada, Y. (1986). *Electron microscopy 1986*, Vol. 1, edited by T. Imura, S. Maruse & T. Suzuki, pp. 29–32. Tokyo: Japanese Society of Electron Microscopy.

Mori, N., Oikawa, T., Katoh, T., Miyahara, J. & Harada, Y. (1988). *Application of the ''imaging plate'' to TEM image recording*. *Ultramicroscopy*, **25**, 195–202.

Reimer, L. (1984). *Transmission electron microscopy*, Chap. 4.6. Berlin: Springer-Verlag.

Schauer, P. & Autrata, R. (1979). *Electro-optical properties of a scintillation detector in SEM*. *J. Microsc. Spectrosc. Electron.* **4**, 633–650.

Valentine, R. C. (1966). *The response of photographic emulsions to electrons*. *Advances in optical and electron microscopy*, edited by R. Barer & V. E. Cosslett, Chap. 5. London: Academic Press.

Zeitler, E. (1992). *The photographic emulsion as analog recorder of electrons*. *Ultramicroscopy*, **46**, 405–416.

7.3

Abele, R. K., Allin, G. W., Clay, W. T., Fowler, C. E. & Kopp, M. K. (1981). *Large-area proportional counter camera for the U.S. National Small-Angle Neutron Scattering Facility*. *IEEE Trans. Nucl. Sci.* **28**(1), 811–815.